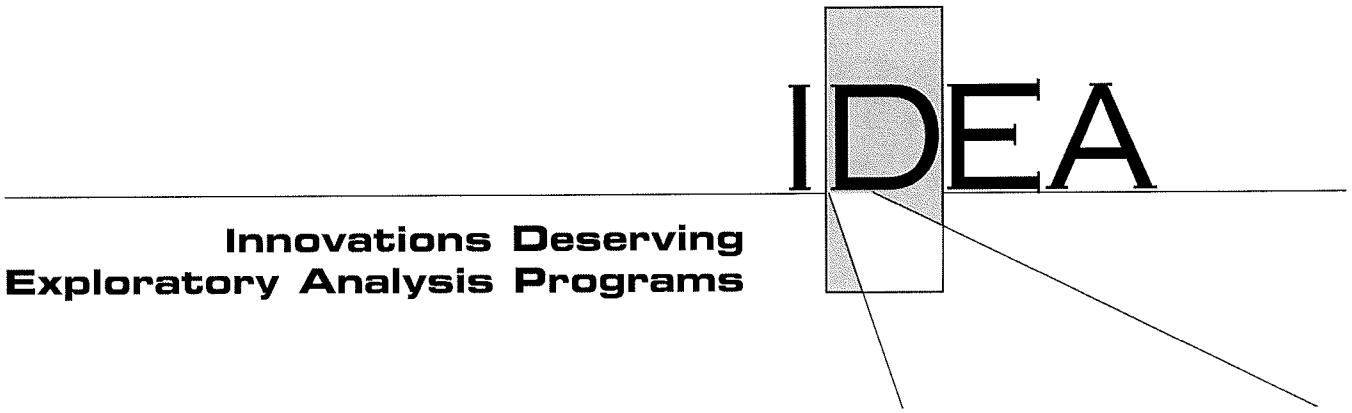

Highway IDEA Program

Active Sensing for Online Highway Bridge Monitoring

Final Report for Highway IDEA Project 120

Prepared by:
Hoon Sohn, Carnegie Mellon University, Pittsburgh, PA

May 2007

TRANSPORTATION RESEARCH BOARD
OF THE NATIONAL ACADEMIES

INNOVATIONS DESERVING EXPLORATORY ANALYSIS (IDEA) PROGRAMS
MANAGED BY THE TRANSPORTATION RESEARCH BOARD (TRB)

This NCHRP-IDEA investigation was completed as part of the National Cooperative Highway Research Program (NCHRP). The NCHRP-IDEA program is one of the four IDEA programs managed by the Transportation Research Board (TRB) to foster innovations in highway and intermodal surface transportation systems. The other three IDEA program areas are Transit-IDEA, which focuses on products and results for transit practice, in support of the Transit Cooperative Research Program (TCRP), Safety-IDEA, which focuses on motor carrier safety practice, in support of the Federal Motor Carrier Safety Administration and Federal Railroad Administration, and High Speed Rail-IDEA (HSR), which focuses on products and results for high speed rail practice, in support of the Federal Railroad Administration. The four IDEA program areas are integrated to promote the development and testing of nontraditional and innovative concepts, methods, and technologies for surface transportation systems.

For information on the IDEA Program contact IDEA Program, Transportation Research Board, 500 5th Street, N.W., Washington, D.C. 20001 (phone: 202/334-1461, fax: 202/334-3471, http://www.nationalacademies.org/trb/idea)

TABLE OF CONTENTS

Active Sensing for Online Highway Bridge Monitoring

Final Report submitted to Transportation Research Board on May 31, 2007

Hoon Sohn, Ph.D.
Civil and Environmental Engineering Department
Carnegie Mellon University
Pittsburgh, PA 15213

1. EXECUTIVE SUMMARY

The objective of this project is to develop an online active sensing system for detecting crack damage on highway bridge systems. In this project, a new "reference-free" nondestructive testing (NDT) technique is being explored so that "certain types of damage can be instantaneously detected without using prior baseline data." This reference-free NDT is based on the concept of a time reversal process (TRP). In the first step, a specific wave form is applied to a lead zirconate titanate (PZT) wafer (PZT A), and the corresponding response is measured at the other PZT wafer (PZT B). Then the measured time response at PZT B is reversed in the time domain and applied back to PZT B. Finally the corresponding response is measured at the original input point, PZT A, and the response is called the "reconstructed" signal in this project. Based on the time reversal concept, it can be shown that the shape of the reconstructed signal should be identical to that of the original input signal as long as the system remains in a linear elastic regime. However, it is expected that the time reversibility will break down if there are nonlinear defects along the wave propagation path. Therefore, by monitoring the deviation of the reconstructed signal from the known input signal, certain types of defects can be detected without direct comparisons with previously obtained baseline signals.

This final report focuses on addressing tasks to be done in Stage 1 and 2. During two stages, the theoretical frame of the proposed baseline-free NDT technique was developed and a NDT methodology for detecting cracks in steel girders commonly used in bridges was formulated. In addition, several field tests at a bridge site in Pennsylvania were conducted to validate the effectiveness of the proposed approach. In particular, this final report attempts to answer to the following specific questions through controlled laboratory experiments as well as field tests. All supporting data and results are provided in the following sections.

I. What is the practical sensing range when the TRP is used for detecting damage? The actual sensing range will be controlled by the magnitude of the input voltage to the active sensing device, the size and thickness of the active sensing device, the material properties of the specimens, driving frequencies, the size and location of our target defect, and so on. Based on the experiments conducted during Stage 1, it is believed that the active sensing system will have a reasonably large sensing range especially compared with the conventional NDT techniques. In the laboratory experiments conducted with a thin aluminum bar specimen, Waves propagating along the thin bar, which is called Lamb waves, generated by the active sensing device were able to propagate up to 40 m. In the field bridge test, it was found that the sensing range of the TRP could be up to 5 to 10 m. However, the sensing range during the actual test was set to around 1 m in order to avoid reflections from the boundaries and stiffeners. Once the effects of these reflections are fully understood, a fewer number of PZTs could be used to inspect a bridge structure.

II. Can different types of flaws be selectively defected and quantified? Stage 1 of this project focused on identifying the presence of crack damage in steel girders. A notch was generated in an aluminum plate to simulate crack damage on a steel girder, and the proposed reference-free NDT technique was applied to detect the crack damage using a piezoelectric transducer pair. The noticeable change due to the crack was observed in the measured reconstructed signal during the TRP: Mode conversion due to crack appeared near the main mode response of the reconstructed signal. This mode converted signals could be successfully extracted from the measured signals when two pairs of PZT transducers are attached on both sides of a plate. From extracted signals, the possible locations of crack damage were determined as well. Additional experiments were conducted to examine if the existence of a foreign object such as the attachment of a steel block could be detected. The attachment of the steel block also affected the reconstructed signal but in a manner different from what was observed from the crack damage. Therefore, it may be feasible to differentiate different types of defects. Additional research is underway to distinguish structural defects from sensor malfunction.

III. How will the sensor conditions affect damage diagnosis? Several experiments were conducted to demonstrate that the debonding and cracking of the active sensing device do not severely affect the TRP used for structural damage detection. Therefore, it is expected that damage diagnosis based on the proposed reference-free NDT technique will not be much affected much by minor sensor defects. However, severe sensor defects will influence the TRP. Therefore, sensor self-diagnosis techniques are also being developed so that the debonding and cracking of the lead zirconate titanate (PZT) wafer used for active sensing can be detected and differentiated from structural damage.

IV. Is damage diagnosis insensitive to undesirable operational and environmental variation of the system? Laboratory experiments are conducted to demonstrate that the proposed NDT technique is not significantly influenced by (1) ambient temperature variations, (2) imperfect sizing and positioning of the active sensing devices, (3) ambient background vibration of the test specimens, (4) changes of the test specimen's boundary conditions, and (5) surface debris or additional painting layers on the steel girders. Field testing results from one of local steel bridges near Pittsburgh clearly demonstrated the robustness of the proposed approach against operational and environmental variations of the bridge.

V. Is the proposed TRP applicable to more complex geometries such as steel girders with stiffeners? For bridge structures, often fatigue cracks are initiated near the connections between the stiffeners and the main girders. Therefore, numerical studies were conducted to investigate the possibility of detecting fatigue crack near the stiffener-girder connection using the proposed reference-free approach. The preliminary results indicate that the proposed approach may be able to detect such crack damage in the stiffener and girder connections. The outcome of the numerical simulations was substantiated by the field testing. However, no destructive test was conducted during the field test, nor the bridge had any prior existing fatigue damage.

In the future, the proposed reference-free NDT technique will be further refined, and the feedback from Transportation Research Board will be incorporated. In order to make technology transition to commercial applications, the following issues will be further investigated.

I. Additional field tests will be conducted at Buffalo Creek Bridge near Pittsburgh to monitor the long term performance of the proposed technique.

II. The automation of the proposed NDT technique will be attempted to minimize costs related to data collection and data interpretation.

III. Practical implementation issues will be investigated so that the proposed system can be used for long term continuous monitoring of field bridges.

2. INTRODUCTION

There has been an increasing demand in using Structural Health Monitoring (SHM) systems for detecting damage within aged civil infrastructures that drive maintenance costs to unprecedented levels. SHM and NDT communities have called for health monitoring for in-situ structures that can query the integrity of structural systems in real time, reducing the need for costly visual inspections, and enabling much more efficient operation and maintenance practices. Conventional studies have focused on schemes where baseline signals are measured so that changes from the baseline can be detected. However, there are significant technical challenges to realizing this vision. For instance, structural defects typically take place several years after the initial baseline data used for compariosn are collected. During this long time period, other operationlal and environmental variatoins of a bridge can produce significant changes in the measured response, masking any potential signal changes due to structural defects.

As an alternative which can overcome the drawbacks of the conventional NDT methods, a concept of a time reversal process (TRP) is adopted to develop a reference-free NDT methodology. The uniqueness of the proposed TRP lies in the premise that "certain types of damage can be instantaneously detected without using prior baseline data." By removing the dependency on the prior baseline data, the proposed damage detection system becomes less vulnerable to operational and environmental variations that might occur throughtout the life span of the bridge structures. Recently, this time reversal concept is being introduced to many applications [1], and its applicability to damage detection has been investigated [2-5].

This report consists of the theoretical explanation of the proposed NDT method and its experimental verification. In this report, the applicability of the time reversal concept to Lamb wave propagation is explained first, and a new method which can extract signals due to damage from the signals after the TRP will be introduced. Then, attention has been paid to significant issues such as (1) sensing range of the proposed TRP, (2) the effects of different types of flaws on the TRP, (3) the effect of sensor bonding condition, and (4) the effects of operational and environmental variations. In section 4, these issues are fully explained and validated experimentally. Once these issues are fully addressed, our vision is to detect certain types of defects on steel bridge structures without relying on any past baseline data.

3. THEORETICAL DEVELOPMENT

In this research, the concept of the TRP is adopted to develop a reference-free NDT methodology for steel bridge structures. The main concept of the TRP is presented briefly and the influence of damage on the TRP is explained. After the definition of damage indices related to the TRP are presented in 3.3, a new method which can extract signals due to damage from the signals after the TRP will be introduced.

3.1 TIME REVERSAL ACOUSTICS FOR BODY WAVES

Body waves are elastic waves that travel through a medium with infinite boundary conditions rather than along an interface. Body waves can be further divided into pressure waves and shear waves. According to time reversal acoustics, an input body wave can be refocused at the source location if a response signal measured at a distinct location is time-reversed (literally the time point at the end of the response signal becomes the starting time point) and reemitted to the original excitation location. An example of time reversal acoustics can also be found in our everyday life: If you would scream "Hello" at the summit of a mountain toward the other side of the mountain, the sound would hit the wall and bounce back at you. Then, you would hear "Hello" echoes. This phenomenon is referred to as time reversibility of body waves and has found applications in lithotripsy, ultrasonic brain surgery, NDT, and acoustic communications [1].

3.2 EXTENSION OF TIME REVERSAL TO LAMB WAVES

The TRP has been widely applied to body waves due to the non-dispersive nature of body waves. However, its application to Lamb waves, which is a wave propagating along thin layers such as steel plates, becomes complicated because of the dispersive and multimode characteristic of Lamb waves [6]. Several researchers have applied the TRP to Lamb wave propagation [7, 8] mainly to refocus the energy of the signal. In this study, the concept of the TRP has been extended to achieve the full reconstruction of the input signal.

An outline of the extended TRP is presented in FIGURE 1. Note that conventional lead zirconate titanate (PZT) materials are employed for generation and sensing of Lamb waves. PZT possesses the property of piezoelectricity, which is the phenomenon of generating an electric charge in a material when subjected to a mechanical stress and conversely generating a mechanical strain in response to an applied electric field. This unique property allows PZT to function as both a sensor and an actuator [9]. First, one PZT patch is designated as an actuator (PZT A), exerting a narrowband tone-burst signal into the structure [FIGURE 1 (a)]. Then, the other PZT (PZT B) becomes a sensor and measures a response signal [FIGURE 1 (b)]. Once the response signal is obtained, the measured signal is reversed in a time domain and reemitted from PZT B to PZT A [FIGURE 1 (c)]. Finally, when the response of the time reversed signal is measured at PZT A again, the energy of the reemitted signal converges to a reconstructed signal [FIGURE 1 (d)]. According to the TRP concept, the shape of the reconstructed signal should be identical to that of the original input signal unless there is nonlinearity induced by damage along a wave path [10]. However, the time reversibility becomes more complex when it is applied to Lamb waves due to the dispersion and multimode characteristics. As shown in FIGURE 1, the reconstructed signal has a main mode and sidebands due to reflections from boundaries and the dispersion and multimode effects of the Lamb waves [3]. Therefore, the deviation of the main mode in the reconstructed signal from the known input signal can be investigated first to check nonlinearity produced by defects. Next, the effect of damage on sidebands can be also investigated in order to identify the existence of damage such as cracks without having reference signals.

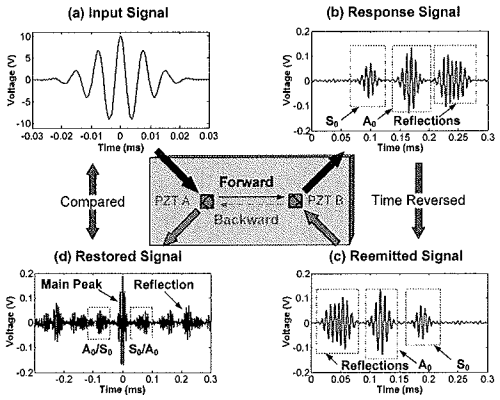

FIGURE 1 A schematic outline of the TRP applied to a plate structure

3.3 DEFINITION OF INDICES FOR NONLINEAR DAMAGE DIAGNOSIS

The indices presented are based on the premise that the reconstructed signal after the TRP will be altered if there is nonlinear damage along a wave propagation path. Currently, two damage indicators are formulated to investigate their sensitivities to damage: time reversibility and symmetry indices. Time reversibility index (TI) is defined so that the difference between the main mode of the reconstructed signal and the original input can be quantified. If two signals are identical, TI becomes zero. As the difference between two signals increases, TI approaches to one.

$$TI = 1 - \sqrt{\left\{\int_{t_l}^{t_r} I(t)V(t)dt\right\}^2 \Big/ \left\{\int_{t_l}^{t_r} I^2(t)dt \int_{t_l}^{t_r} V^2(t)dt\right\}} \tag{1}$$

where $I(t)$ and $V(t)$ are denoting the input signal and the main mode of the reconstructed signal, respectively. t_l and t_r are the starting and ending points of the main mode. Next, Symmetry Index (SYMI) is proposed to determine the symmetry of the reconstructed signal after the TRP:

$$SYMI = 1 - \sqrt{\int_{t_0}^{t_r} \{R(t)L(-t)\}^2 dt} \Big/ \sqrt{\int_{t_0}^{t_r} R^2(t)dt \int_{t_l}^{t_0} L^2(t)dt} \tag{2}$$

where $R(t)$ and $L(t)$ are the right and left sides of the reconstructed signal, respectively. t_0, t_l and t_r are the starting and ending times of the referencing range of the SYMI. The definition of each term in Eq. (2) is illustrated in FIGURE 2. It can be shown that when a symmetric input signal is applied, the reconstructed signal should be also symmetric. However, the presence of nonlinear damage is expected to break down the symmetry of the reconstructed signal.

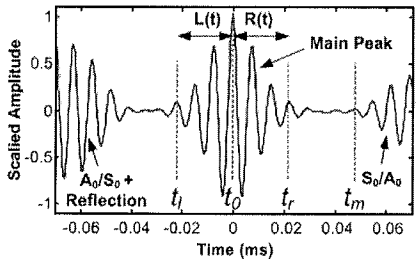

FIGURE 2 Definition of $L(t)$, $R(t)$, t_l, and t_r

3.4 THE EFFECT OF MODE CONVERSION ON THE TRP

According to the TRP concept, the TRP will not be achieved at the presence of nonlinear damage [10]. However, in homogeneous elastic materials such as steel plates, the nonlinearity produced by the notch may not affect the reconstructed signal much that the shape of the main mode in the reconstructed signal can be preserved. Therefore, more attention is paid to sidebands due to the mode conversion in order to detect crack damage in metallic structures such as steel girders. In this report, a concept of using the polarization characteristic of piezoelectric materials is proposed to extract mode converted signals in the reconstructed signal after the TRP. In the following section, the basic understanding of piezoelectric materials and the effect of their polarization characteristic on Lamb wave propagation is investigated first.

3.5 PIEZOELECTRIC MATERIAL AND ITS POLARIZATION CHARACTERISTICS

Piezoelectric materials are natural or artificially polarized ceramics which have piezoelectricity [11]. These materials develop an electrical charge or voltage when a mechanical pressure is applied, which is the simplest description of piezoelectricity. Conversely, piezoelectric materials produce deformation (strain) when exposed to an applied electric field. Due to this unique nature of the piezoelectric materials, they are commonly used as both sensors and actuators in many applications [12]. For instance, wafer-type piezoelectric materials such as PZT are commonly used for exciting and measuring guided waves for SHM and NDT applications [9]. In some natural ceramic materials such as quartz, crystal cells, which behave similarly to electric dipoles, are oriented along the crystal axes. However, artificially polarized materials must be poled to have piezoelectricity due to the random orientation of the dipoles at the initial state [11]. In order to force piezoelectricity to the materials, a thermal treatment is commonly utilized. In the first stage, a crystalline material with randomly oriented dipoles is slightly warmed up below its Curie temperature [FIGURE 3 (a)]. After strong electric field E is applied to the crystalline material, the dipoles in the material align along the field lines [FIGURE 3 (b)]. Finally, the material is cooled down, and the electric field is removed [FIGURE 3 (c)]. The polarization of the material is permanently maintained as long as the poled material stays below its Curie temperature. The overall behavior of a piezoelectric material as well as its electrical characteristics is governed by the poling direction of the material (Buchanan, 2004). In the next section, the influence of the poling direction on Lamb waves is discussed.

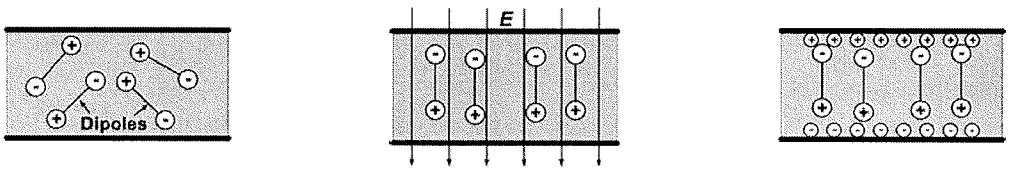

(a) A crystalline material is heated up near its Curie temperature

(b) The applied electric field aligns the dipoles along the field lines

(c) The polarization is permanently maintained after cooling

FIGURE 3 A poling process of an artificially polarized material [11]

3.6 THE EFFECT OF PZT POLING DIRECTIONALITY ON LAMB WAVE PROPAGATION

In this section, it is investigated how the phase of a Lamb wave mode changes depending on (1) the poling directions of exciting and sensing PZT wafer transducers and (2) whether a wafer transducer is attached either on the top or bottom surface of a plate. For illustration, it is assumed four identical PZT wafer transducers, labeled as "A", "B", "C, and "D",

are attached to a plate as shown in FIGURE 4 (a). The arrows indicate the positive poling directions of each PZT transducers. PZTs A and D are placed exactly at the same position but on the other side of the plate. PZTs B and C are positioned in a similar fashion. Furthermore, it is assumed that a narrow-band tone burst signal is applied as an input, and the driving frequency is chosen such that only the fundamental symmetric (S_0) and anti-symmetric (A_0) modes are generated.

When PZT A is excited, the S_0 and A_0 modes are generated and measured at PZTs B and C [6]. In an ideal condition, the amplitude and arrival time of the S_0 mode measured at PZTs B and C should be identical. In addition, both PZTs B and C should be subjected to positive bending because of the symmetric nature of the S_0 mode (See the figure on the left in FIGURE 4 (b)). (In this paper, this term of "positive bending" is used when the positively polarized side of the PZT is subjected to tensile strain. On the other hand, the PZT is subjected to negative bending when the negatively polarized size of the PZT is subjected to tensile strain. The positive bending produces a "positive" output voltage while the negative bending results in a "negative" output voltage value.) Because both PZTs B and C are subject to the positive bending, the phase of the S_0 mode measured at these PZTs are identical as well as the amplitude and arrival time (See the S_0 mode in FIGURE 6 (a)). As far as the A_0 mode is concerned, PZT B is subjected to the negative bending although PZT C still undergoes the positive bending (See the figure on the right in FIGURE 4 (b)). Therefore, the A_0 modes measured at PZTs B and C are out-of-phase (See the A_0 mode in FIGURE 6 (a)). However, when the poling direction of the PZT C is switched [FIGURE 5 (a)], PZTs B and C will produce out-of-phase S_0 modes and in-phase A_0 modes [FIGURE 5 (b) and FIGURE 6 (b)].

This idea of using the PZT poling directionality in Lamb wave propagation is not a completely new idea. However, the majority of the past work has focused on selective generation of S_0 and A_0 modes [13]. For instance, by exciting PZTs A and D shown in FIGURE 4 (a) in-phase, only the S_0 mode can be excited. In this study, the polarization characteristic of the PZT is utilized not only for selective generations of Lamb wave modes but also for selective measurements. In the following section, this concept is further advanced so that the mode conversion due to crack formation can be extracted from the measured Lamb wave signals.

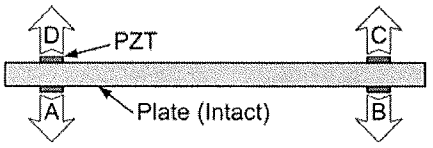

(a) Test configuration I with collocated PZTs with the opposite poling directions

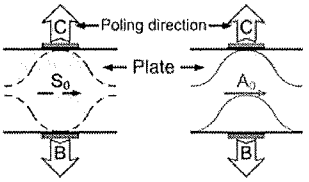

(b) The S_0 mode produces the same bending for PZTs B and C while the A_0 mode results in the opposite bending.

FIGURE 4 The effect of the PZT poling directions on the phases of the S_0 and A_0 modes (Configuration I)

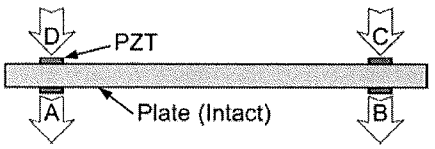

(a) Test configuration II with all PZTs with the same poling directions

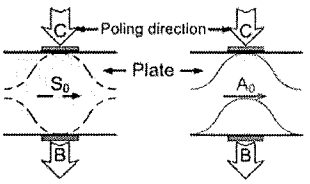

(b) The S_0 mode produces the opposite bending for PZTs B and C while the A_0 mode results in the same bending.

FIGURE 5 The effect of the PZT poling directions on the phases of the S_0 and A_0 modes (Configuration II)

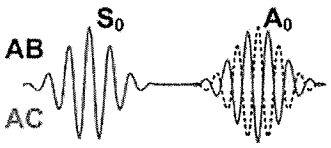

(a) S_0 and A_0 modes measured from configuration I in FIGURE 4 (a): S_0 modes in-phase & A_0 modes out-of-phase

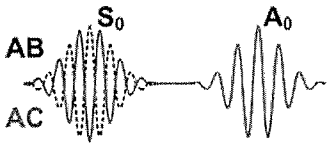

(b) S_0 and A_0 modes measured from configuration II in FIGURE 5 (a): S_0 modes out-of-phase & A_0 modes in-phase

FIGURE 6 A schematic comparison of the S_0 and A_0 modes measured from Configurations I and II shown in FIGURE 4 (a) and FIGURE 5 (a), respectively: AB (a dash line) and AC (a solid line) denote the response signals measured at PZTs B and C when a tone burst input is applied at PZT A.

3.7 EXTRACTING MODE CONVERTED SIGNALS DUE TO CRACK DAMAGE USING A PZT POLING DIRECTION

In this subsection, the PZT polarization characteristic is further advanced so that the mode conversion due to crack formation can be detected without using any prior baseline data. First, the effect of a crack on Lamb wave modes is described. If Lamb waves propagating along a thin plate encounter a discontinuity, some portion of the waves are reflected at the discontinuity point and others are transmitted through it. When a S_0 mode arrives at the notch as shown in FIGURE 7, it is separated into S_0 and A_0 modes (denoted as S_0/S_0 and A_0/S_0, respectively). In a similar manner, an A_0 mode is also divided into S_0 and A_0 modes (S_0/A_0, and A_0/A_0). This phenomenon is called mode conversion [14].

When the plate is in a pristine condition and four identical PZTs are instrumented as shown in FIGURE 8 (a), it can be shown that a signal AB becomes identical to a signal CD as illustrated in FIGURE 8 (b) [15]. Here, the signal AB denotes the response signal measured at PZT B when the excitation is applied at PZT A, and the signal CD is defined in a similar fashion. However, the signal AB is no longer identical to the signal CD [FIGURE 8 (c) and (d)] when there is a crack between PZTs A and B (or PZTs C and D). As for the signal AB, the S_0/A_0 mode arrives at PZT B earlier than the A_0/S_0 mode when the notch is located closer to PZT A than PZT B (assuming that the S_0 mode travels faster than the A_0 mode). Conversely, the S_0/A_0 mode arrives at PZT D later than the A_0/S_0 mode in the case of the signal CD. In FIGURE 8 (d), the signals AB and CD are drawn considering not only the arrival time of each mode but also the poling directions of the PZTs. While the S_0 and A_0 modes in FIGURE 8 (d) are in-phase, the S_0/A_0 and A_0/S_0 modes in the signals AB and CD are fully out-of-phase. Therefore, the additional modes generated by a notch can be extracted simply by subtracting the signal AB from the signal CD as shown in FIGURE 8 (d). Also, note that this approach can be applied to the comparison between signals AC and BD. In the next section, this idea is extended to the proposed TRP, and the effect of mode conversion on the TRP is closely investigated.

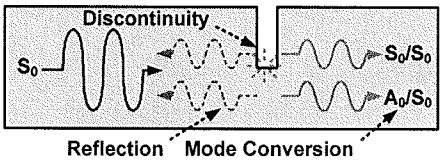

FIGURE 7 A schematic diagram of mode conversion and reflection due to a discontinuity on a plate

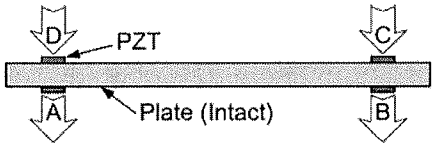

(a) An intact plate with the PZT configuration II shown in FIGURE 5 (a)

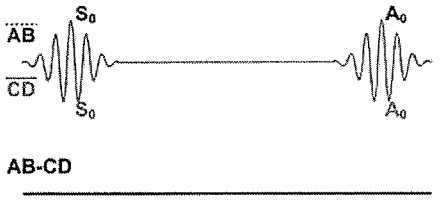

(b) Comparison of signals AB and CD without a notch: the S_0 & A_0 modes are identical

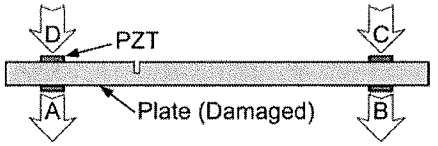

(c) A damaged plate with the PZT configuration II shown in FIGURE 5 (a)

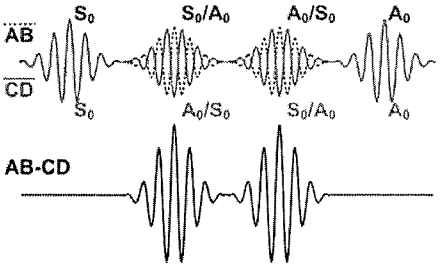

(d) Comparison of signals AB and CD with a notch: the S_0 & A_0 modes are identical, but the S_0/A_0& A_0/S_0 modes are out-of-phase

FIGURE 8 Extraction of the additional Lamb wave modes generated by a notch using the poling directionality of the PZT transducers (A_0/S_0 mode denotes an A_0 converted from S_0 when it passes through a crack. S_0/A_0 is defined similarly.)

3.8 THE APPLICATION OF THE DAMAGE DETECTION TECHNIQUE TO THE TRP

Finally, the new crack damage detection technique is applied to the TRP. The proposed TRP has several advantages over the direct Lamb wave comparison technique. It was shown experimentally that the size effect and bonding effect which affects direct Lamb wave signals can be compensated by using TRP, and the TRP is also proven to be more robust to the environmental and operational variations than direct Lamb wave signals [15]. However, the TRP produces sidebands around its main mode due to the multimodal characteristic of Lamb waves and the effect of boundaries [3], which makes it complicated to analyze reconstructed signals after the TRP. In FIGURE 9, a brief schematic diagram of the TRP is shown. Here, a signal ABA denotes a reconstructed signal after a TRP starting from PZT A and ending at the PZT A again. A signal CDC is defined in a similar fashion. If there is no damage along a wave path, there will be only a main mode and two sidebands (in solid boxes) due to mode coupling. Once a notch is generated, Lamb wave signal AB or CD is divided into four modes, and each mode creates four modes again while the TRP is conducted. For the TRP, forwarding signal is truncated right after the arrival of an A_0 mode. Ultimately, total 16 modes are combined to generate a reconstructed signal as shown in FIGURE 9. Here, note that the main mode and two side bands will be in-phase with or without damage. However, two out-of-phase signals (in dashed boxes) will appear with respect to the damage. Therefore, the existence of a defect can be determined by observing out-of-phase signals similarly to the Lamb wave cases. This idea is experimentally validated in Chap 4.

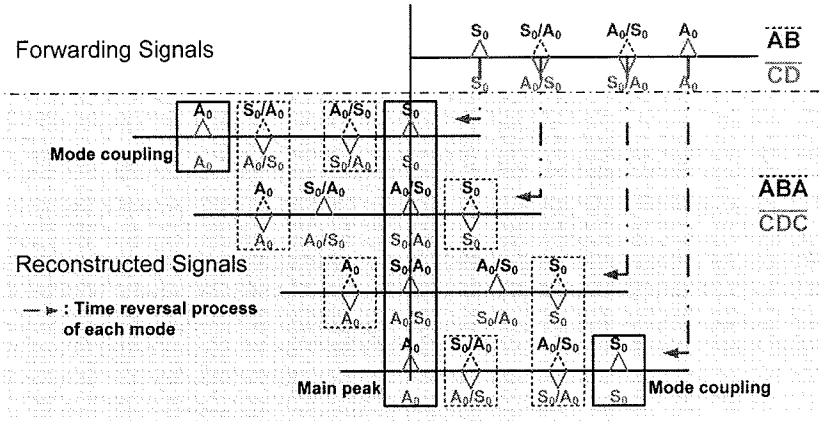

FIGURE 9 A brief description of a time reversal process in Lamb wave propagation

3.9 DEVELOPMENT OF A THRESHOLDING TECHNIQUE TO ADDRESS VARIATIONS IN PZT SIZE, ALIGNMENT AND BONDING CONDITION

In the previous subsection, it is shown that the signals AB and CD (or ABA and CDC) are indistinguishable when there is no crack [FIGURE 8 (b)]. This is based on the assumption that all PZT transducers are identical and PZTs A and D (or PZTs B and C) are perfectly collocated. In practice, these assumptions can not be fully satisfied because of variations in PZT size, alignment and bonding condition [15]. Therefore, residual differences would remain after subtracting the two signals even at the absence of crack, and this could be a source of positive false alarms. To tackle this practical implementation issue, a thresholding technique is developed in this subsection.

The development of this signal processing technique is based on the observation that the additional modes generated by a crack are out-of-phase while the other modes are in-phase when signals AB and CD are compared [FIGURE 8 (d)]. According to FIGURE 8 (d), because S_0 modes and A_0 modes in signals AB and CD are in-phase, the point by point product (PPP) values between not only S_0 modes but also A_0 modes are always positive. On the other hand, the PPP between S_0/A_0 (A_0/S_0) in the signal AB and A_0/S_0 (S_0/A_0) in the signal CD produces negative values. Therefore, the existence of a crack can be detected by observing the negative PPP values between the signals AB and CD. Note that this idea can be also applied to a reconstructed signal case such as ABA and CDC comparison. Then, it is investigated how the PPP values are affected by variations in PZT size, alignment and bonding condition. The main effects of the non-ideal PZTs on the signals AB and CD can be summarized as the amplitude change of the response signals and the time shifting of one signal with respect to the other. For instance, the debonding and/or cracking of PZT A can reduce the coupling area between PZT A and the substrate and consequently decrease the amplitude of the signal AB with respect to the signal CD. It can be readily shown that this pure amplitude change does not alter the negative PPP values to the positive values and vice versa. However, the variations in PZT size, alignment and bonding condition can also cause phase shifting, and this requires a special treatment.

In FIGURE 10, an example of the phase shift caused by PZT transducer misalignment is illustrated. The results shown in FIGURE 10 are obtained from the same configuration shown in FIGURE 5 (a) except that PZT C is shifted 0.76 mm to the right with respect to PZT B. That is, the distance between PZTs A and B becomes 0.76 mm shorter than the distance between PZTs C and D. Due to this misalignment, the A_0 mode in the signal CD is delayed about 0.25 μs with respect to the A_0 mode in the signal AB (0.76 mm / 3.055 mm/μs = 0.25 μs) [FIGURE 10 (a)]. Because the A_0 mode travels slower

than the S_0 mode at 150 kHz (V_S = 5.088 mm/μs, V_A = 3.055 mm/μs), the A_0 mode is more severely affected by the misalignment than the S_0 mode. Therefore, the discussion here focuses on the delay of A_0 modes. Furthermore, note that 0.76 mm misalignment is equivalent to 8 % of the 10 mm× 10 mm PZT wafer transducer size. Although 0.25 μs may be considered a small time delay, FIGURE 10 (b) shows that this time delay produces a substantial difference between the signals AB and CD when they are subtracted from each other.

On the other hand, FIGURE 10 (c) shows that the PPP values between the signals AB and CD are mostly positive except at a few negative points. The negative PPP values are the results of the misalignment and amplified in FIGURE 10 (d). It can be analytically shown that the PPP between the two signals at 150 kHz produces a 300 kHz frequency component as shown in FIGURE 10 (c). Therefore, the time period of the PPP values becomes 3.33 μs (= 1/300 kHz). The observation of FIGURE 10 (d) further reveals that the duration of the negative PPP values is shorter than that of the positive PPP values. For instance, 3 mm misalignment, which is equivalent to 30 % misalignment in a 10 mm× 10 mm PZT wafer transducer, produces 0.98 μs (= 3 mm / 3.055 mm/μs) duration of the negative PPP values. Note that the mode conversion also produces negative PPP values. However, the duration of the negative PPP values caused by the mode conversion becomes 2.35 μs (= 3.33 μs – 0.98 μs) in this configuration. Therefore, the duration of the negative PPP values due to the mode conversion remains longer than the duration caused by PZT misalignment as long as the PZT misalignment is controlled under certain precision. In this paper, it is assumed that the PZT misalignment can be controlled under 30 % of the 10 mm× 10 mm PZT transducer size and this misalignment produces 0.98 μs duration of the negative PPP values. Then, the effect of the misalignment is eliminated by removing the negative PPP values, whose duration is less than 0.98 μs [FIGURE 10 (e)]. The effectiveness of this thresholding technique is further investigated in Chap. 4.

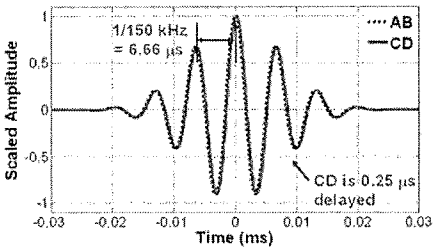

(a) Signals AB and CD when PZT C is shifted 0.76 mm to the right with respect to PZT B

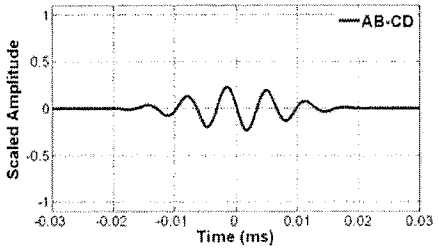

(b) Difference between signals AB and CD

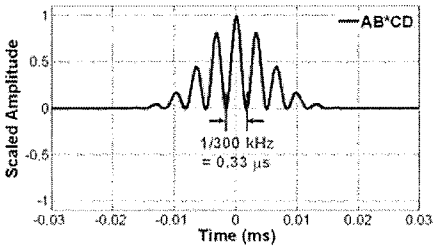

(c) The PPP values between signals AB and CD when PZT C is shifted 0.76 mm to the right wrt. PZT B

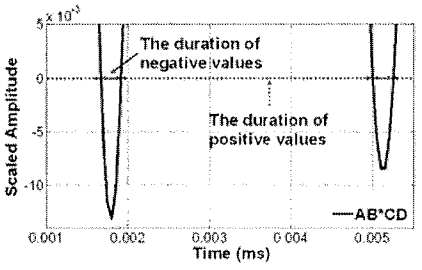

(d) Zoomed-in version of (c), indicating the durations of positive values and negative values due to misalignment

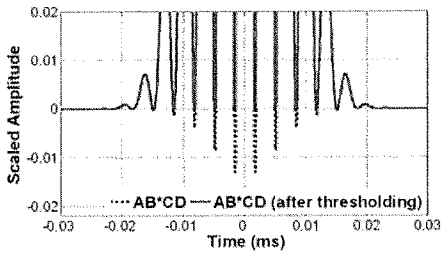

(e) Zoomed-in version of (c), highlighting the negative values of the PPP:
a dash line – before thresholding, and a solid line – after thresholding

FIGURE 10 Compensation of sensor misalignment using the proposed thresholding process
(AB*CD denote the point-by-point product (PPP) between signals AB and CD)

4. PRACTICAL ISSUES RELATED TO IMPLEMENTATION OF THE PROPOSED REFERENCE-FREE NDT SYSTEM

The final objective of this research is to develop a NDT technique which is applicable to real bridge structures. In order to achieve this goal, there are several practical implementation issues needed to be answered first. In this section, the sensing range of the TRP and the effects of different types of flaws, bonding conditions, environmental and operational variations on the TRP and the Lamb wave propagation in a complex geometry were investigated through numerical simulation and laboratory experiments.

4.1 WHAT IS THE PRACTICAL SENSING RANGE WHEN THE TRP IS USED FOR DETECTING DAMAGE?

The practical sensing range of the proposed NDT technique is closely related to the travel distance of Lamb waves because the Lamb waves created at the excitation point should be measurable at the sensor location which is away from the excitation location. To study the sensing range in a metallic structure, Lamb wave propagation characteristics along a thin aluminum plate was examined. A pair of 1 cm × 1 cm PSI-5A4E PZTs (thickness = 0.0508 cm) was mounted on an aluminum bar (182.88 cm × 10.16 cm × 1.27 cm). The distance between these two PZTs was 152.4 cm (5'). A maximum 10 V signal was exerted to a PZT at 50 kHz, and the received signal was magnified ten times using a low noise signal amplifier. FIGURE 11 (a) shows Lamb waves along the direct wave propagation paths and ones reflected from the boundaries. Even after 0.015 sec, the amplitudes of Lamb waves were above the background noise level. Considering that the S_0 and A_0 mode velocities are 5,231 m/s and 2,960 m/s at 50 kHz, it is calculated that the reflected Lamb waves are still measurable using our data acquisition system even after traveling over 40m. FIGURE 11 (b) shows that the TRP was achieved successfully in this test.

Note that, there are several factors which affect the propagation distance of Lamb waves such as the magnitude of the input voltage, the PZT size and thickness, the material properties and thickness of the medium, the driving frequency and the complexity of the structure. The Lamb waves can propagate a longer distance when the input voltage level and PZT thickness increase because a higher voltage or a thicker PZT can generate larger strain to the structure. Also, Lamb wave can propagate more distance along a thinner medium typically. After the voltage level and PZT thickness is determined, the optimal PZT size and driving frequency can be determined with respect to the material properties and thickness of the medium [16]. However, the sensing range of the TRP can be limited due to the complex geometry of the steel girder

structures in practice. In a 1-D wave propagation case, there are only 2 boundaries where waves are reflected from. If a 3-D structure such as a girder structure is considered, reflections from the edges of the web as well as flanges can influence the TRP, which may limit the sensing range of the TRP within 5 to 10 m. Therefore, several ideas related to the reflection problems are now being investigated and verified prior to real girder tests.

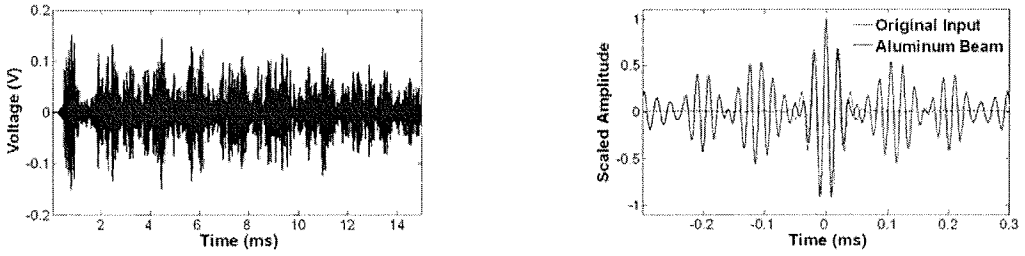

(a) Forwarding signal (b) Reconstructed signal after the TRP

FIGURE 11 Signals from an aluminum beam

4.2 CAN DIFFERENT TYPES OF FLAWS BE SELECTIVELY DETECTED AND QUANTIFIED?

This research intends to detect and monitor the initiation and growth of defects within steel girders. In particular, the primary goal of this study is to detect crack damage along the steel girders. In this section, it is investigated how two different types of defects affect the TRP. For the first damage case, a small piece of steel block was attached on one surface of an aluminum plate. The second damage case was simulated by introducing a notch on the test structure surface. These two damage cases were investigated using a 4ft-by-4ft aluminum plate further described in the following section. It was observed that the two damage cases investigated differently affected the time reversibility.

4.2.1 Test Setup

The overall test configuration is shown in FIGURE 12 (a). To verify the proposed TRP and the damage diagnosis method, experimental studies has been conducted on an aluminum plate [FIGURE 12 (a) and (b)]. The dimension of the plate is 122 cm× 122 cm× 0.6 cm, and two PZT patches, which are 0.52 m apart each other, are mounted in the middle of the plate. The test setup consists of an arbitrary waveform generator (AWG), a high-speed signal digitizer (DIG), a low noise preamplifier (LNP) and an aluminum plate specimen [FIGURE 12].

A tone-burst signal in a range of 20 peak-to-peak voltage is generated using a 14-bit arbitrary waveform generator, and the PZTs are excited at the frequency of 90 KHz and 130 KHz. First, PZT A in FIGURE 12 (b) is excited by this input waveform. Then, PZT A generates elastic waves and the response is measured at PZT B. In this experiment, a PSI-5A4E type of PZT (thickness = 0.0508 cm) is cut to 1 cm by 1 cm and attached to the surface of the plate with a commercial cyanoacrylate adhesive.

When the waves arrive at PZT B, the voltage output from PZT B is amplified 10 times using the low noise preamplifier and measured by DIG. The sampling rate of DIG is 5 MS/sec, and resolution is 16 bits. The total length of the recorded signal is set to 0.22 ms (after the arrival of the direct A_0 mode) for damage test. Once the signal is recorded, the signal is reversed in the time domain and saved as a new input signal. This new input is applied to PZT B, and the response is

measured at PZT A. Then, the reconstructed signal acquired at PZT A is compared with the original tone-burst input signal. The effect of flaws on the reconstructed signal is discussed in the following section.

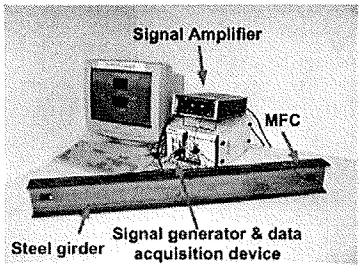

(a) A testing configuration

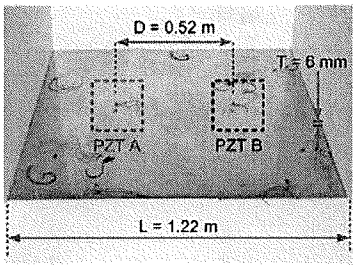

(b) A square aluminum plate

FIGURE 12 Testing configuration for detecting defects on an aluminum plate

4.2.2 Damage Type I: Foreign Objects along a Wave Path

First, damage was simulated by attaching a steel block along the wave propagation path as presented in FIGURE 13. A steel block of 5.0 cm × 4.5 cm × 0.6 cm was attached in the middle of PZTs A and B. For the TRP, only the first arrivals of S_0 and A_0 modes have been reversed (t = 0.22 ms). In this way, the contribution of reflections to the TRP has been removed.

If Lamb waves propagating along a thin plate encounter a discontinuity such as thickness change, some portion of the waves are reflected at the discontinuity point and others are transmitted through it [FIGURE 7]. Furthermore, the transmitted waves can be converted into other types of modes and this is called mode conversion [13]. The effects of the mode conversion on the forwarding response signal and the reconstructed signal are illustrated in FIGURE 7.

Two noticeable changes are observed in FIGURE 14 (a). First, the amplitudes of S_0 and A_0 modes were reduced due to the block attached between PZTs A and B. In particular, the A_0 mode has been more severely influenced by the attachment of the block than the S_0 mode. Second, the shapes of S_0 and A_0 modes also have been altered. It is suspected that the shape changes are caused by a combination of mode conversion and reflection at the block location. Although the attenuation itself did not change the time reversibility of the reconstructed signal, the combined effect of the mode conversion and reflection from the block seemed to degrade the time reversibility. FIGURE 14 (b) shows the distortion of the time reversibility due to the block attachment.

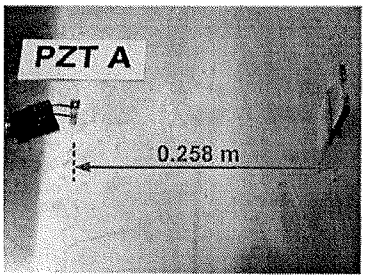

FIGURE 13 A steel block (5.0 cm H × 4.5 cm W × 0.6 cm T) attached between PZT A and B

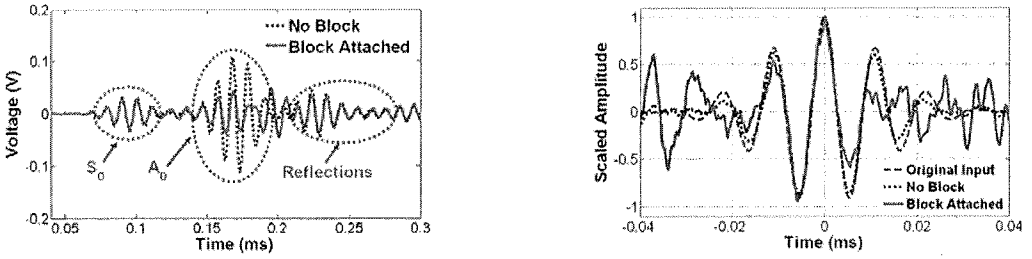

(a) A forward signal measured at PZT B (b) A reconstructed signal at PZT A

FIGURE 14 The effects of block attachment on the forward and the reconstructed signal at 90 kHz

4.2.3 Damage Type II: Notches along a Wave Path (1) – TRA (Experimental Results)

Next, a notch was introduced between PZT A and B to simulate a crack as shown in FIGURE 15. Physically, a crack behaves differently from a notch because the crack keeps opening and closing depending on loading condition. However, the NDE technique in this report aims to monitor steel bridge structures under changing operational variation. When monitoring is conducted without blocking traffic, a fatigue crack might experience continuous opening and closing. When the crack is opening, it is expected that the behavior of the opened crack will be similar to that of a notch. All the experimental conditions of this damage case were identical to the type I damage case except for the simulated defect. The appearance of mode conversion due to the notch is shown in FIGURE 16. When the S_0 mode encounters a notch, it is separated into the S_0 and A_0 modes, which are denoted as S_0/S_0 and A_0/S_0. Similarly, A_0 is divided into two modes, S_0/A_0 and A_0/A_0. Based on the arrival time of the A_0 and S_0 modes, their group velocities are estimated to be 5.163 m/ms and 3.025 m/ms at 130 kHz. Then, the arrival times of additional modes due to mode conversion at the notch location (S_0/A_0 and A_0/S_0) are estimated to be 0.135 ms. Because the notch was introduced exactly in the middle of the two PZTs, two additional modes, S_0/A_0 and A_0/S_0, arrived at the same time. These estimated arrival times match well with those of the additional modes observed in FIGURE 16 (a), confirming that these are, in fact, additional modes produced by mode conversion. However, the mode conversion due to the notch changed time reversibility very little as shown in FIGURE 16 (b). It is expected that because the notch does not necessarily introduce nonlinearity in the test specimen, the time reversibility is not affected by the notch. However, it should be noted that sidebands (the additional modes shown inside of the dotted box in FIGURE 16 (b)) are generated near the main mode response.

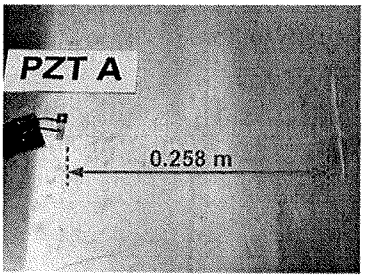

FIGURE 15 A notch of 8 cm (W × 0.2 cm T × 0.3 cm D) between PZTs A and B

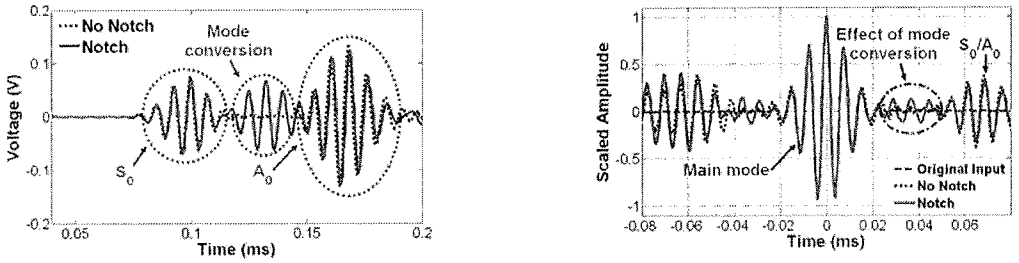

(a) A forward signal measured at PZT B (b) A reconstructed signal at PZT A

FIGURE 16 Mode conversion introduced by notch (exciting frequency at 130 kHz)

The objective of this report is to examine the effect of notch or crack on the proposed TRP and the applicability of the proposed TRP to more complex geometries such as steel girders with stiffeners. In order to achieve this goal, the TRP in thin metal plates and stiffener-girder connections are closely examined by numerical simulation. After the simulation, the TRP in metal plates were investigated through laboratory experiments.

4.2.4. Damage Type II: Notches along a Wave Path (2) – Using the PZT Polarization Characteristic (Numerical Simulation)

In 4.2.2 and 4.2.3, the distortion of a main mode in a reconstructed signal due to a foreign object between two transducers was observed [FIGURE 14 (b)]. In addition, the effect of mode conversion on the TRP was clearly shown when a notch was generated along a wave path [FIGURE 16 (b)]. However, the shape of the reconstructed signal's main mode did not alter in spite of the mode conversion. Instead, the mode converted signals appeared as sidebands. Therefore, a damage detection technique in 3.3, which uses the poling direction of the piezoelectric materials to extract mode converted signals, is closely investigated in 4.2.4 and 4.2.5.

The idea of using a PZT poling direction for crack detection was first validated by numerical simulation. For simplicity, the numerical simulation is conducted for direct Lamb wave propagation cases only. Using COMSOL Multiphysics software (www.comsol.com), Lamb wave propagation in a two dimensional aluminum beam was simulated using the combination of plain strain, piezo plain strain, and electrostatics modules in COMSOL software. The length of the beam was 70 cm, and its thickness was 6 mm. Four identical PZTs with a size of 10 mm × 10 mm × 0.508 mm were attached to the beam model as shown in

FIGURE 17. Note that PZTs A and D were collocated but on the other side of the beam with the same poling direction. PZTs B and C were placed in a similar fashion. The parameter values used in the numerical simulation are listed in TABLE 1. A narrowband tone-burst signal at 150 kHz frequency was used as an input signal. In the simulation, Rayleigh damping coefficients were set to 10^{-4} for a mass damping coefficient and 0 for a stiffness damping coefficient, respectively. The simulation results were obtained from a time dependent solver, and a time step was set to 0.25 μs, which is equivalent to 4 M samples/sec. To control the error in each integration step, relative tolerance and absolute tolerance for the solution were chosen to be 10^{-3} and 10^{-10}, respectively. The maximum backward differentiation formula (BDF) order for setting the degree of the interpolating polynomials in the time-stepping method was set to order 2. Finally, the model was meshed using a mapped mesh option, and the size of each mesh was limited to 1 mm × 1 mm. [17]

FIGURE 18 illustrates that signals AB and CD were almost identical and this well corresponds to the theoretical expectation. Once a notch of 3 mm depth and 1 mm width was introduced 100 mm away from PZT D toward PZT C, the signal AB became different from the signal CD as a result of the mode conversion induced by the crack [FIGURE 19 (a)]. The mode conversion due to cracking was extracted simply by subtracting the signal CD from the signal AB [FIGURE 19 (b)].

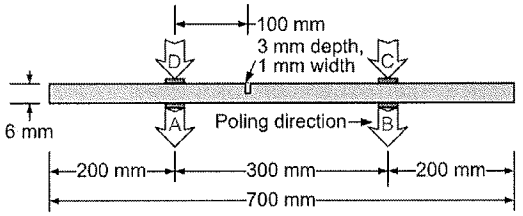

FIGURE 17 Dimension of an aluminum plate used in numerical simulation

TABLE 1 Parameters used in numerical simulation

Exciting frequency	150 kHz
α (Mass damping coeff.)	10^{-4}
β (Stiffness damping coeff.)	0
Sampling rate	4 Ms/s
Relative tolerance	10^{-3}
Absolute tolerance	10^{-10}
Maximum BDF order	2
Mesh size (mapped mesh)	1 mm× 1 mm max.

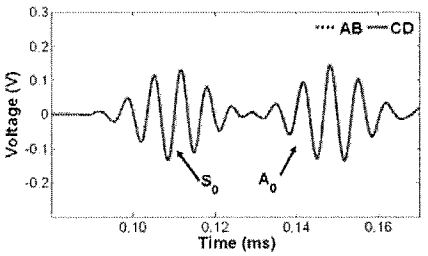

(a) Signals AB and CD without a notch

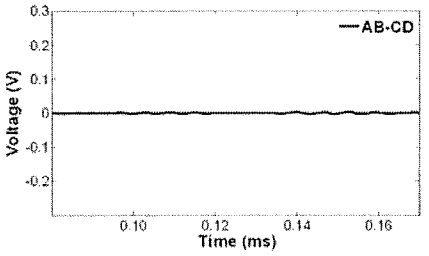

(b) Difference between signals AB and CD

FIGURE 18 Simulated Lamb wave signals without notch

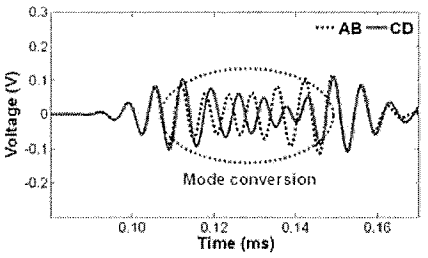

(a) Signals AB and CD with a notch (3 mm depth, 1 mm width)

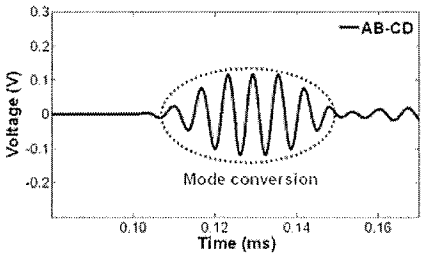

(b) Difference between signals AB and CD with a notch (3 mm depth, 1 mm width)

FIGURE 19 Simulated Lamb wave signals with a notch of 3 mm depth and 1 mm width

So far it has been assumed that all PZTs are identical, and two PZTs on the both sides of the beam are precisely collocated. In practice, the size, bonding condition and electrical impedance of a PZT transducer will vary from one device to another, and there can be PZT misalignment. To investigate the effectiveness of the proposed thresholding techniques for addressing these practical implementation issues, the previous numerical simulation was repeated after introducing misalignment between PZTs B and C: PZT C was shifted 1 mm to the right with respect to PZT B. Although the shapes of the signals AB and CD were almost identical as shown in FIGURE 20 (a), their subtraction produced residuals, whose amplitudes were much higher compared to the one in FIGURE 18 (b) [FIGURE 20 (b)]. FIGURE 21 (a) shows the PPP values between the signals AB and CD, and the negative PPP values were magnified in FIGURE 21 (b).

By determining the duration of the negative PPP values and removing negative values whose duration is less than the threshold value (0.98 μs defined in Section 2.4.), the effect of the PZT misalignment was removed in FIGURE 21 (b).

In FIGURE 22 (a), the numerical simulation was repeated again with a crack introduced at 100 mm away from PZT A toward PZT B as well as the PZT misalignment. Subtracting the signals AB from the CD produced the residual signal shown in FIGURE 22 (b). Without relying on prior baseline data, it is challenging to determine whether this remaining signal appears due to mode conversion or sensor misalignment. However, by calculating the PPP between signals AB and CD and applying the proposed thresholding technique, the mode conversion due to crack was extracted as shown in [FIGURE 23 (a) and (b)]. This numerical example demonstrates that crack can be identified even when there is PZT transducer misalignment. This finding is further substantiated in the following experimental study.

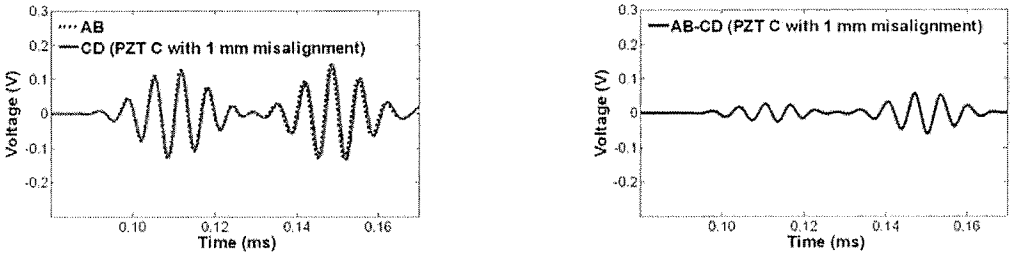

(a) Signals AB and CD with PZT C shifted 1 mm to the right wrt PZT B

(b) The difference between signals AB and CD with PZT C shifted 1 mm to the right wrt PZT B

FIGURE 20 The effect of PZT misalignment on the difference between signals AB and CD
(PZT C shifted 1 mm to the right with respect to PZT B)

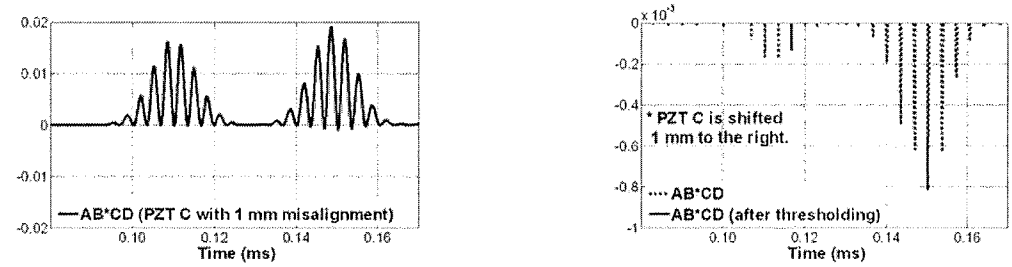

(a) The PPP values between signals AB and CD when PZT C is shifted 1 mm to the right wrt to PZT B

(b) Negative PPP values between signals AB and CD before and after applying the proposed thresholding

FIGURE 21 Compensation of the PZT transducer misalignment using the proposed thresholding technique
(PZT C: shifted 1 mm to the right with respect to PZT B, without a notch)

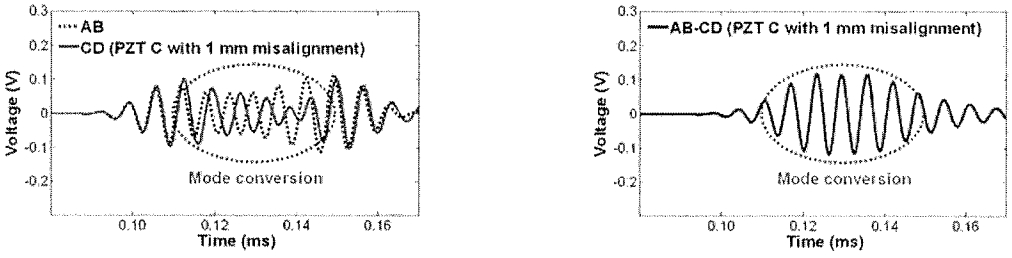

(a) Signals AB and CD with PZT C shifted 1 mm to the right and a 3 mm depth notch

(b) Difference between signals AB and CD with PZT C shifted 1mm to the right and a 3 mm depth notch

FIGURE 22 Comparison of signals AB and CD with PZT transducer misalignment and a 3 mm depth notch

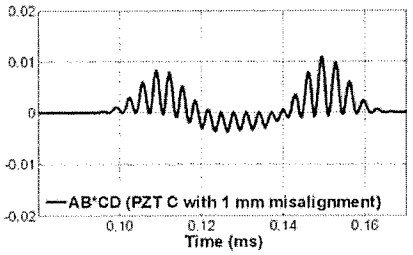

(a) The PPP values between signals AB and CD with PZT C shifted 1 mm to the right and a 3 mm depth notch

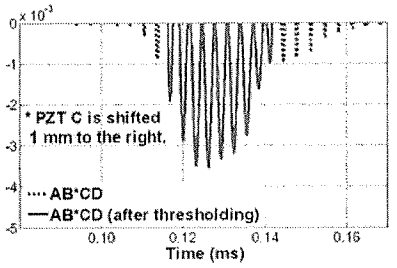

(b) Negative PPP values between signals AB and CD before and after applying the proposed thresholding

FIGURE 23 The extraction of the mode conversion using the proposed thresholding technique at the presence of the PZT transducer misalignment (PZT C: shifted 1 mm to the right with respect to PZT B and a 3 mm depth notch)

4.2.5. Damage Type II: Notches along a Wave Path (3) – Using the PZT Polarization Characteristic (Experimental Results)

To further examine the proposed reference-free NDT technique described in 3.4 through 3.9, experimental tests have been conducted on an aluminum plate again. All the test parameters and test configuration are identical to the ones in 4.2.3 except for exciting frequency and the LNP gain (Exciting frequency = 150 kHz, LNP gain = 20). Note that four PSI-5A4E type PZT wafer transducers (1.0 cm× 1.0 cm× 0.0508 cm) were mounted in the middle of the plate. PZTs A and D were collocated and attached on the other side of the plate, and PZTs B and C were mounted in a similar fashion. The PZTs were attached so that their poling directions were identical to the configuration shown in **Error! Reference source not found.** (a). PZTs A and B (or PZTs C and D) were 0.52 m apart each other. In this experiment, the PZT transducers were attached to either the top or the bottom surface of the plate with commercial cyanoacrylate adhesive.

In this experiment, after the forwarding signal from PZT A to PZT B (signal AB) was measured, the same process was repeated by exciting PZT C and measuring response at PZT D (signal CD). Finally, the PPP values of signals AB and CD were calculated, and the negative PPP values due to sensor misalignment were selectively removed. The entire experimental process without averaging signals took less than 15 Seconds. After forwarding Lamb wave signals are measured, the TRP is conducted. The signal AB (signal CD) was reversed in a time domain, and resent to the PZT B (PZT D). The reconstructed signal after the TRP was created at PZT A (PZT C) location, and the signal ABA was compared with signal CDC as is done in signal AB and CD case. Detailed test results are described in the next subsection.

In FIGURE 25 (a), Lamb wave signals obtained from an intact plate are presented. Using the test setup described in 4.2.1, signals AB and CD were measured. Although the signal AB was supposed to be identical to the signal CD, a residual signal was observed in FIGURE 25 (b) due to imperfections in PZT alignment, size and bonding condition.

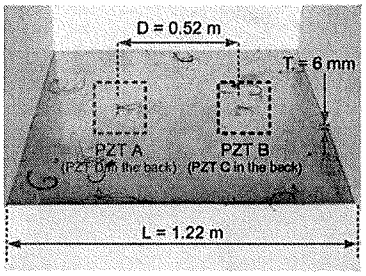

FIGURE 24 Testing configuration for detecting a crack on an aluminum plate

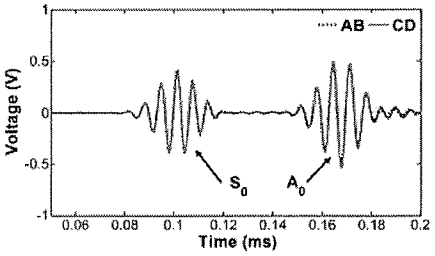

(a) Signals AB and CD without notch

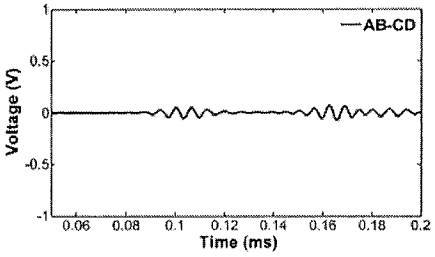

(b) Difference between signals AB and CD

FIGURE 25 Comparison of signals AB and CD without notch

Next, a 3 mm (depth) × 1 mm (width) × 60 mm (length) notch was introduced between PZTs A and B (or PZTs C and D). The notch was located 150 mm away from PZT A toward PZT B. As a consequence, two additional modes due to the mode conversion appeared between the existing S_0 and A_0 modes as shown in FIGURE 26 (a). Comparison of FIGURE 25 (b) and FIGURE 26 (b) shows the mode conversion effect on the difference between the signals AB and CD. Then, the proposed thresholding technique was applied to the PPP values between the signals AB and CD before and after introducing crack. Using the proposed thresholding technique, the negative PPP values resulted from the mode conversion were retained while the negative values associated with the sensor misalignment were selectively removed. As shown in FIGURE 27 (a), the negative PPP values between signals AB and CD was negligible at the absence of a notch. Once the notch was introduced, the effect of the two additional modes clearly appeared as shown in FIGURE 27 (b). The arrival times of these two additional modes well correspond to the theoretical calculation.

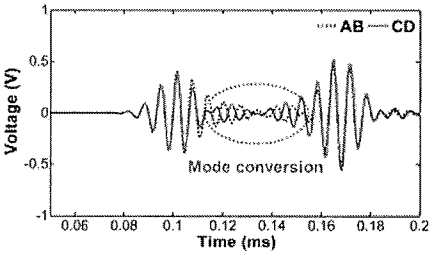

(a) Signals AB and CD with a 3 mm notch

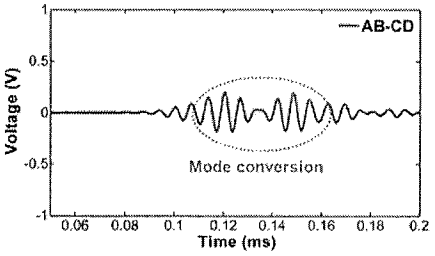

(b) Difference between signals AB and CD

FIGURE 26 Comparison of signals AB and CD with a 3 mm depth notch

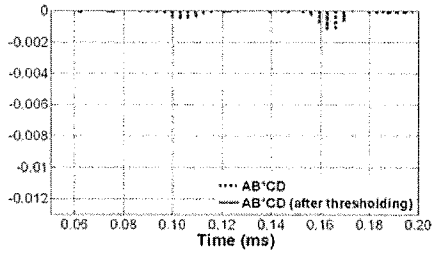

(a) Negative PPP values between signals AB and CD before and after applying the proposed filtering (without a notch)

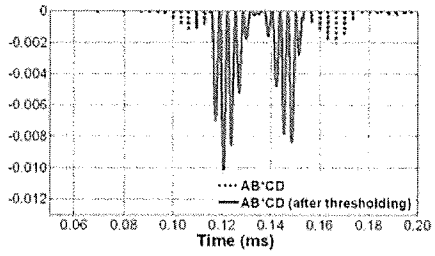

(b) Negative PPP values between signals AB and CD before and after applying the proposed filtering (with a 3 mm depth notch)

FIGURE 27 The extraction of the mode conversion produced by a 3 mm depth notch using the proposed filtering technique at the presence of the PZT transducer misalignment

Note that possible locations of the notch can be estimated by measuring the arrival times of two additional modes in signals AB and CD. According to the signal AB in FIGURE 25 (a), the velocity of the S_0 and A_0 modes were estimated to be 5.128 m/ms and 3.099 m/ms (theoretically, V_S = 5.088 m/ms and V_A = 3.055 m/ms), respectively. The location of a notch is closer to PZT A than PZT B when the S_0/A_0 mode (S_0 converted from A_0) arrives earlier than the A_0/S_0 mode (A_0 converted from S_0). Conversely, when the A_0/S_0 arrives earlier than the S_0/A_0, the notch is close to B. However, it is impossible to determine whether the first arrived mode converted signal is S_0/A_0 or A_0/S_0 in signals AB and CD because both S_0/A_0 mode and A_0/S_0 modes are in-phase in the signal AB and are out-of-phase in the signal CD [FIGURE 8 (d)]. Therefore, two possible notch locations are determined assuming that the location can be closer to either the PZT A or the PZT B. Assuming the notch is closer to the PZT A, the distance from A to the notch can be estimated using Eq. (3) based on a velocity-distance relationship:

$$\text{The arrival time of the first mode conversed signal} = \frac{s}{V_a} + \frac{\text{Distance between PZT A and PZT B - s}}{V_s} \tag{3}$$

where V_a, V_s, and s denote the velocity of A_0 mode, the velocity of S_0 mode, and the distance of notch from A, respectively. By observing the arrival time of the first mode (0.1206 ms) and using Eq. (3), the two possible locations of the notch were estimated to be at 15.03 cm away from PZT A or PZT B. This estimated distance was almost identical to the actual distance (0.2 % difference) from the PZTs. Here, two notch locations are indicated using an AB and CD combination. It is also possible that the exact notch location can be determined including other signals such as a signal AC and a signal BD. For instance, the signals AB and AC have out-of-phase S_0/A_0 signals and in-phase A_0/S_0 signals. Therefore, from the negative PPP values between signals AB and AC, the arrival time of the S_0/A_0 signal can be determined. Once the arrival time of S_0/A_0 is known, whether the notch is close to PZT A or PZT B can be decided that the exact damage location is finally estimated. Later, this idea of pinpointing exact notch location will be validated by including other PZT combinations.

Finally, same procedure was conducted using a reconstructed signal after the TRP. As explained previously, two noticeable peaks appeared after a notch was made. The existence of damage is clearly indicated by comparing FIGURE 30 (a) and (b). Note that the location of the damage can be also estimated by the arrival time of two additional modes in the reconstructed signal. As shown in FIGURE 9, the possible locations of the notch can be determined by checking the arrival time of the first mode converted signal in the reconstructed signal. The arrival time of the first mode converted signal in the reconstructed signal matches with the difference between the first mode converted signal and the S_0 signal in direct Lamb wave signals. In this case, the arrival time of the first mode converted signal in the reconstructed signal was 2.065×10^{-5} sec. Then, two possible locations of the notch are estimated to be at 16.17 cm away from PZT A or PZT B (7.8 % difference).

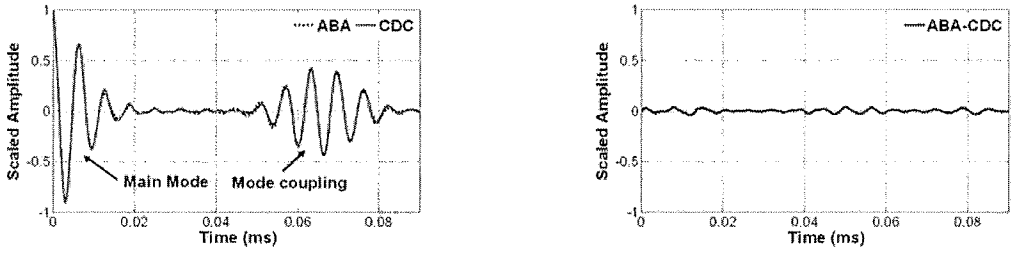

(a) Signals ABA and CDC without notch (b) Difference between signals ABA and CDC

FIGURE 28 Comparison of signals ABA and CDC without notch

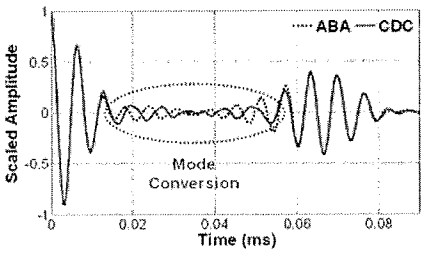

(a) Signal ABA and CDC with 3 mm notch

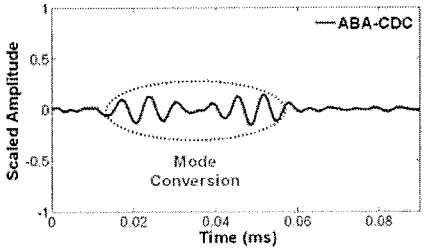

(b) Subtraction of signal CDC from signal ABA

FIGURE 29 Comparison of signals ABA and CDC with a 3 mm depth notch

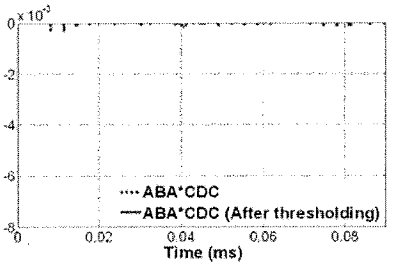

(a) Negative PPP values between signals ABA and CDC before and after applying the proposed filtering (without a notch)

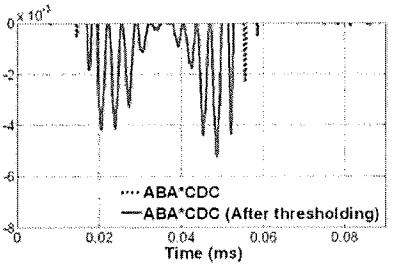

(b) Negative PPP values between signals ABA and CDC before and after applying the proposed filtering (with a 3 mm depth notch)

FIGURE 30 Negative values of reconstructed signals ABA and CDC

In summary, it is observed that the attachment of the steel block and the notch have characteristically different effects on the time reversibility. Based on this difference, it may be feasible to distinguish different types of defects. Currently different types of damage indices are being developed to detect and classify various types of defects. However, the primary interest for steel bridges will be crack damage. In the future, a method which can pinpoint crack location and differentiate crack damage from sensor malfunction will be investigated as well.

4.3 HOW WILL THE SENSOR CONDITION AFFECT DAMAGE DIAGNOSIS?

Lamb waves generated by the PZT devices will be directly affected by the bonding condition between the PZT and the structure. Therefore, the sensing system would have to be recalibrated if current Lamb-wave based damage detection systems were deployed for scheduled periodic maintenance. In addition, the gradual degradation of the sensor bonding condition would have an adverse effect on damage diagnosis for a long term continuous monitoring. Although it is expected that the proposed baseline-free technique would be less susceptible to the sensor bonding condition, it can still be influenced by severe sensor failure.

Recently, the TRP is also applied to detect PZT wafer debonding and cracking [18]. Lee and Sohn (2006) applied the concept of the TRP to a single PZT. First, an input signal is applied to the single PZT, and the response reflected off from the boundaries is measured at the same PZT. Then, the measured response signal is reversed in the time domain and applied back to the PZT. Similar to the TRP with two PZTs, the reconstructed signal corresponding to this reversed signal should be identical to the original input signal. Sensor failure such as debonding is detected by measuring the deviation of

the reconstructed signal from the original input signal. In addition, a Non-Linearity (NL) index is proposed to detect PZT cracking:

$$NL = \sqrt{\frac{1}{M}\sum_{k=0}^{M}\left(\frac{V_1[k]-K\cdot V_2[k]}{V_1[k]}\right)^2} \tag{4}$$

where $V_1[k]$ and $V_2[k]$ denote the discrete version of the first output signal and the second output signal up to M data points with two different input levels in terms of the magnitude, K is the magnitude ratio of the first input signal to the second input signal, and, M is the number of total data points. This index is based on the premise that if there is cracking on the PZT wafer, the time response of the output signal is not linearly proportional to that of the input signal in terms of the magnitude [19]. For instance, $V_1[k]$ and $V_2[k]$ are assumed to be measured data using 1 V and 10 V input voltage, respectively. In a linear system, a tenfold input voltage will amplify the output ten times. However, when nonlinearity such as sensor cracking happens in the system, $V_2[k]$ can not be 10 times higher than $V_1[k]$. The proposed NL is formulated based on this idea, and the NL index becomes zero if two output signals are exactly linearly proportional and increases if they are not exactly proportional.

The possible reason why the PZT cracking increases the NL index is that the impulse can be created between the gap of the crack of the PZT wafer when the PZT wafer vibrates. This undesired motion is the source of the nonlinearity of the system under the continuous excitation. For the test, normal PZT condition case is compared with debonding and cracking condition cases shown in FIGURE 31 using a prototype sensor circuit [FIGURE 32] and a specimen in [FIGURE 33].

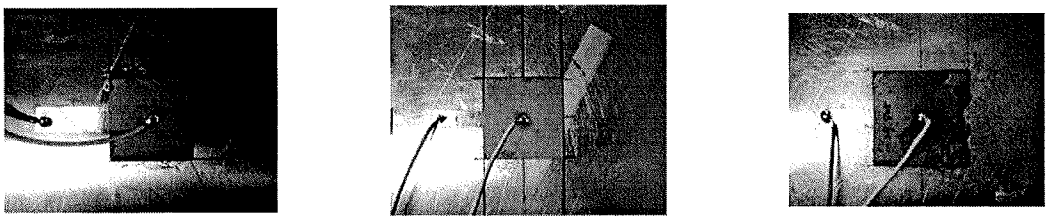

(a) Normal condition (b) Debonding condition (c) Cracking condition

FIGURE 31 Three different conditions of the PZT wafer

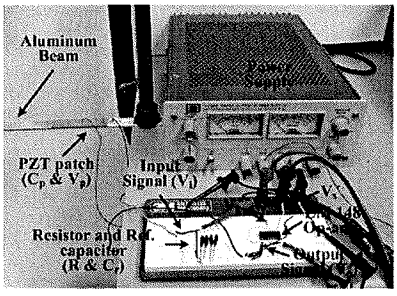

FIGURE 32 A prototype of the self-sensing circuit

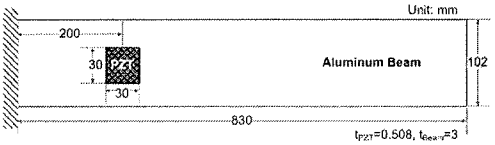

FIGURE 33 Dimensions of the test structure and the PZT wafer

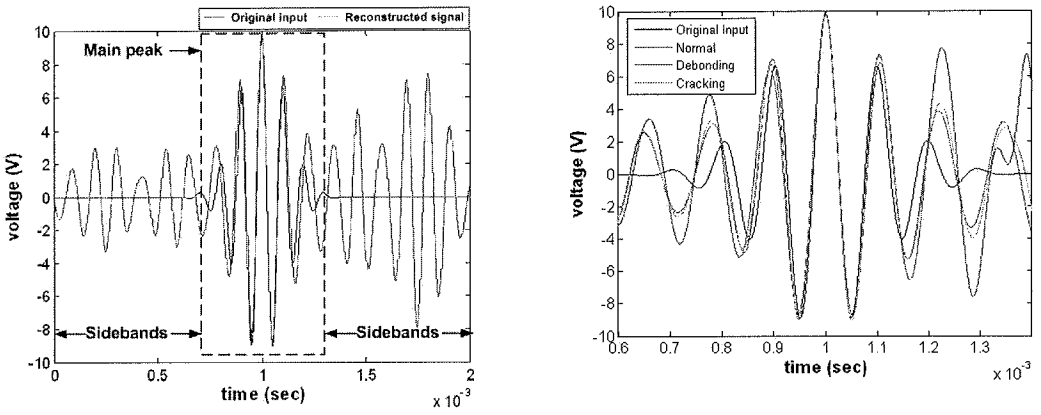

FIGURE 34 Reconstructed signals in different sensor conditions

TABLE 2 Quantitative results of the proposed features for the beam structure

PZT condition / Features	Normal	Debonding (about 25%)	Cracking (about 20%)
TI	0.0902	**0.2439**	0.1134
SYMI	0.0043	**0.0368**	0.0082
NL	1.9362×10^{-5}	1.1449×10^{-5}	**1.0540×10^{-4}**

The test results are shown in FIGURE 34 and TABLE 2. From the result, sensor debonding could be differentiated from normal condition using TI and SYMI. Even though sensor cracking was not determined using TI and SYMI as shown in TABLE 2, a large increase of NL distinguished sensor cracking from the normal condition of PZT. The sensor diagnosis methodology presented in this section is now being developed and verified with the damage detection technique proposed in this report.

4.4 IS DAMAGE DIAGNOSIS INSENSITIVE TO UNDESIRABLE OPERATIONAL AND ENVIRONMENTAL VARIATION OF THE SYSTEM?

To deploy a monitoring system for in-situ bridges, the monitoring system should be robust against operational and environmental variations in order to minimize false-alarming of damage. In this section, several operational and environmental parameters of a test specimen are varied to demonstrate that the proposed reference-free NDT technique is robust against these variations.

As shown in FIGURE 35, a 119 cm × 5.08 cm × 0.6 cm aluminum bar is used in this experiment because of its simplicity. The rest of the test setups are identical to the ones described in section 4.2 except for the exciting frequency (150 kHz).

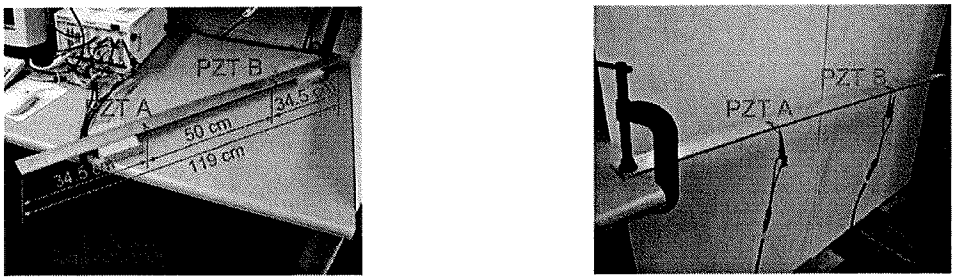

(a) Simply supported (b) One end fixed

FIGURE 35 An aluminum bar specimen used for tests

4.4.1 Effect of Temperature Variation on the TRP

In-situ steel bridge structures are often subjected to daily and seasonal temperature variations. It should be noted that the temperature variation can change the material property and boundary condition of the bridge as well as the properties of the sensors. In return, they introduce changes in the measured response signals. Therefore, developing a NDT technique which is robust to temperature variation is of great importance in order to prevent false-positive alarming of damage.

In this section, the influence of varying temperature on the TRP was investigated. First, the aluminum bar with 2 PZT sensors was tested after it was refrigerated to -20 °C (-4 °F). Next, the middle part of the aluminum bar including PZTs was heated to 40 °C (104 °F). Then, the results from two cases were compared with room temperature (26 °C (79 °F)) test case.

The responses corresponding to the two different temperature conditions are shown in FIGURE 36 (a) and FIGURE 37 (a), respectively. These are the forwarding signals measured at PZT B when the input signal is applied to PZT A. While the amplitude changes were negligible, a noticeable phase shift of the response signal was observed. The temperature increase seems to decrease the wave propagation speed. However, it was observed that the temperature variation did not significantly affect the TRP because the TRP automatically compensated the phase shift of the forwarding signal during its time reversal procedure. Since temperature variation mainly causes the phase shift, the shape and symmetry of the reconstructed signal are preserved even in the presence of the temperature variation [FIGURE 36 (b), FIGURE 37 (b), TABLE 3]. Therefore, it is expected that daily and seasonal temperature variations of a bridge structure will not affect the proposed reference-free NDT technique.

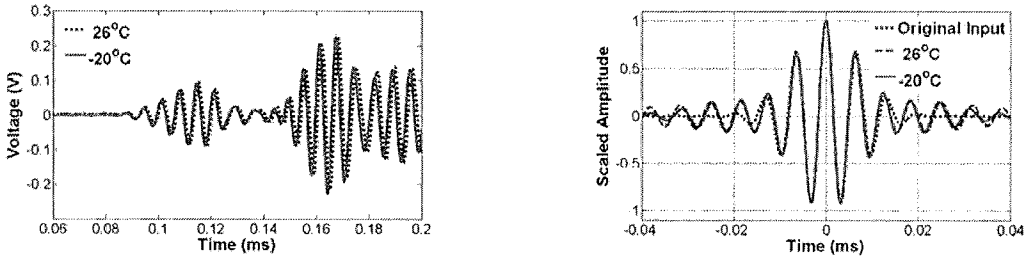

(a) Forwarding signal (b) Reconstructed signal after the TRP

FIGURE 36 Comparison between medium and low temperature cases

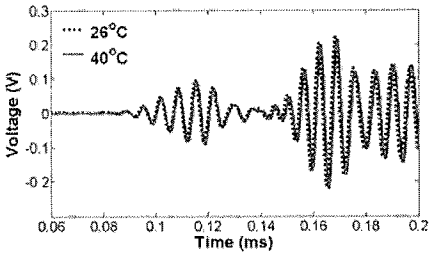

(a) Forwarding signal

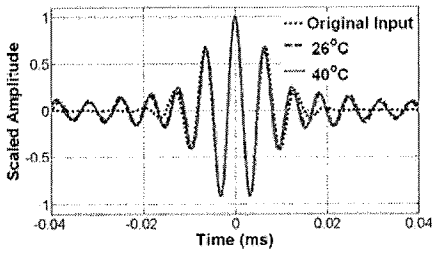

(b) Reconstructed signal after the TRP

FIGURE 37 Comparison between medium and high temperature cases

TABLE 3 Damage Indices in Different Temperature Cases

Degree	TI	SYMI
-20 °C	0.0249896	0.994325
26 °C	0.0207283	0.999920
40 °C	0.0372928	0.999685

4.4.2 Effect of Imperfect PZT Sizing

In the theoretical development of the TRP, it is assumed that the two PZTs used for the TRP are identical. In this section, the effect of the PZT size difference on reciprocity and time reversibility was examined. For the reciprocity and time reversal results presented in FIGURE 38, a 1.0 cm× 1.0 cm PZT was used at location A and a 0.7 cm× 0.7 cm PZT was attached at location B. The observation of FIGURE 38 (a) revealed that the amplitudes of signals AB and BA were different although the response shapes were still very similar. In particular, the amplitude of the response signal was higher when the input was applied to the larger PZT (PZT A) than to the smaller one (PZT B). However, the different sizes of the PZTs did not affect time reversibility as illustrated in FIGURE 38 (b).

Next, the size difference between PZT A and B has been increased. In the experiment shown in FIGURE 39, the size of PZT B was increased to 2.0 cm× 2.0 cm while the size of PZT A remained to be 1.0 cm× 1.0 cm. A pattern similar to FIGURE 38 was observed. However, the amplitude of signal BA was higher than that of signal AB in FIGURE 39 (a) because a larger PZT was used at location B. In addition, the phase shift of the time reversal signal became noticeable in FIGURE 39 (b). It is speculated that this phase shift is due to the size difference of the PZTs. For the calculation of the TR index in Eq. (1), the phase shift can be compensated before computing the TR index. Further investigation is warranted to quantitatively relate the phase shift amount with the PZT size difference.

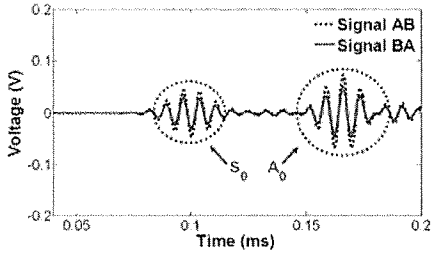

(a) Reciprocity for signals AB and BA

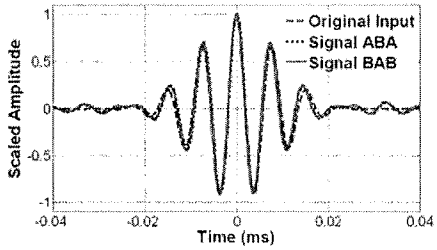

(b) Time reversibility for signals ABA and BAB

FIGURE 38 The effect of PZT size on reciprocity and time reversibility
(PZT A: 1.0 cm × 1.0 cm, PZT B: 0.7 cm × 0.7 cm, 130 KHz, t = 1 ms reversed)

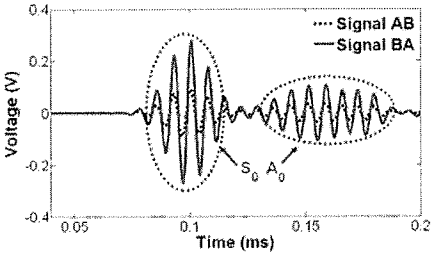

(a) Reciprocity for signals AB and BA

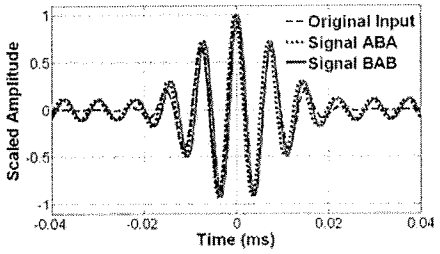

(b) Time reversibility for signals ABA and BAB

FIGURE 39 The effect of PZT size on reciprocity and time reversibility

(PZT A: 1.0 cm × 1.0 cm, PZT B: 2.0 cm × 2.0 cm, 130 KHz, t = 1 ms reversed)

4.4.3 Effect of PZT Orientation and Shape

In this section, the effect of the PZT orientation and shape difference on reciprocity and time reversibility was investigated. For the reciprocity and the TRP tests, three different test sets were prepared [FIGURE 40]. For all cases shown in FIGURE 40, the PZTs on the right side of the plate (PZT A) were designed to have a square shape (1 cm × 1 cm) and the shapes of the PZTs on the other side of the plate (PZT B) were varied from a rectangle shape (2 cm × 0.5 cm) to an equilateral triangle of 1.52 cm side and a square (1 cm × 1 cm) with 45 degree rotation. Note that all PZTs have the same area (1 cm^2). Even though the shape and amplitude of each forwarding signals in FIGURE 41, FIGURE 42, and FIGURE 43 (a) were different from each case, the shape difference of the PZTs did not distort time reversibility as presented in FIGURE 41, FIGURE 42, and FIGURE 43 (b). According to the results in 4.4.2 and 4.4.3, it can be inferred that the reciprocity of Lamb wave propagation can be preserved without regard to the area and shape of each PZT.

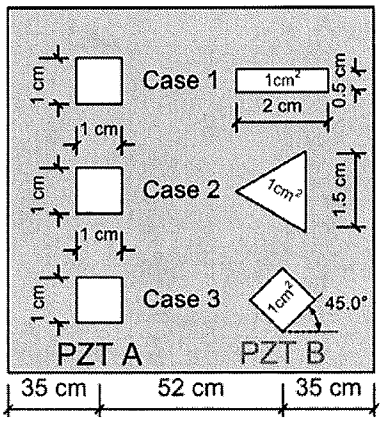

FIGURE 40 Sensors in different orientation and shapes.

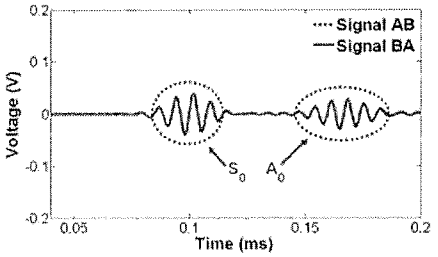

(a) Reciprocity for signals AB and BA

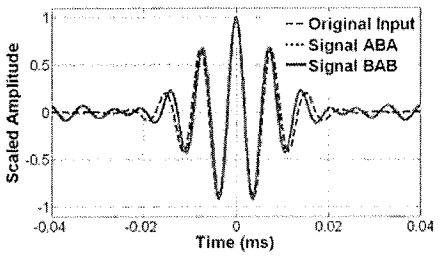

(b) Time reversibility for signals ABA and BAB

FIGURE 41 The effect of PZT Shape on reciprocity and time reversibility in Case 1

(PZT A: 1.0 cm× 1.0 cm, PZT B: 2.0 cm× 0.5 cm)

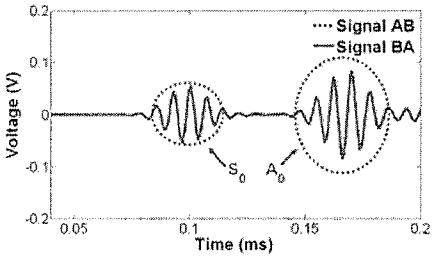

(a) Reciprocity for signals AB and BA

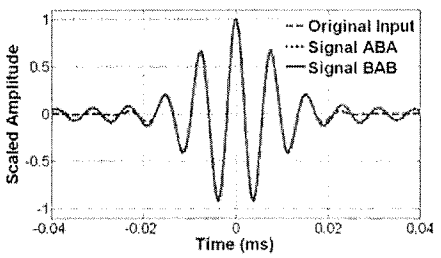

(b) Time reversibility for signals ABA and BAB

FIGURE 42 The effect of PZT Shape on reciprocity and time reversibility in Case 2

(PZT A: 1.0 cm× 1.0 cm, PZT B: An equilateral triangle with 1.52 cm side)

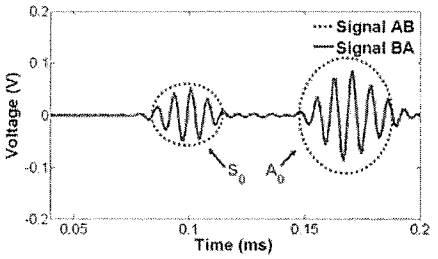

(a) Reciprocity for signals AB and BA

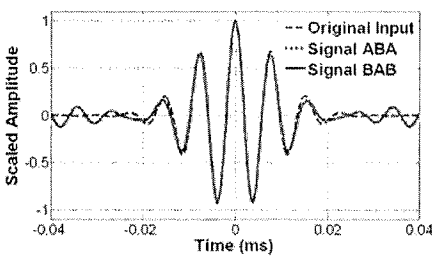

(b) Time reversibility for signals ABA and BAB

FIGURE 43 The effect of PZT Shape on reciprocity and time reversibility in Case 3

(PZT A, B: 1.0 cm× 1.0 cm, PZT B is 45° rotated with respect to PZT A)

4.4.4 Effect of the Boundary Condition of the Structure on the TRP

The robustness of the proposed method against changing boundary conditions was investigated using the two different configurations shown in FIGURE 35. In FIGURE 35 (a), the beam was laid on top of two wooden blocks. In FIGURE 35 (b), the one end of the beam was fixed using a clamp. FIGURE 44 (a) shows the forwarding and reconstructed signals obtained from these two configurations. It was observed that the boundary condition change affected the Lamb wave modes reflected from the clamped edge of the bar as shown in FIGURE 44 (a). However, it is shown that the damage and symmetry indices will be invariant of the varying boundary conditions [FIGURE 44 (b), TABLE 4].

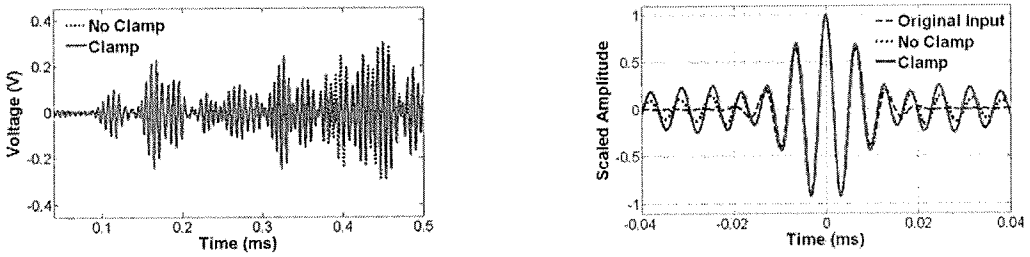

(a) Forwarding signal (b) Reconstructed signal after the TRP

FIGURE 44 Comparison between no clamp and clamp cases

TABLE 4 Damage Indices in Different Boundary Conditions

	TI	SYMI
No Clamp	0.0207283	0.999920
Clamp	0.0239801	0.999513

4.4.5 Effect of Ambient Vibrations on the TRP

Due to normal traffic on in-situ bridge structures, the vibration responses of the bridges are often dominated by traffic loading. Therefore, it is very difficult to single out the guided wave responses generated only by the active sensing device at the presence of more predominant vibration responses due to traffic. Although filtering can minimize the effect of traffic-induced vibrations, their effects cannot be completely removed.

In this section, the effect of ambient vibrations on the reciprocity and time reversibility was investigated. In order to simulate background noise or ambient vibration, one end of an aluminum bar was tapped about 4 times per second (4 Hz) by a steel ruler. As is shown in FIGURE 45 (a), the tapping produced a draft in signal AB, and this draft remained even after applying a bandpass filter in the range of 3 kHz to 1 MHz. After the TRP, the effect of ambient vibration still existed that the reconstructed signal showed low frequency fluctuation. However, the effect of the tapping was not shown much in the zoomed-in reconstructed signal of FIGURE 45 (b). It is speculated that the frequency of the fluctuation is much lower than the exciting frequency that its effect is not clearly seen when the reconstructed signal is zoomed in to see only main mode. The *TI* and *SI* values summarized in TABLE 5 show that the main mode of the reconstructed signal was not affected much by additional loading. In this section, it was illustrated that the effect of ambient loading on the TRP is minimal.

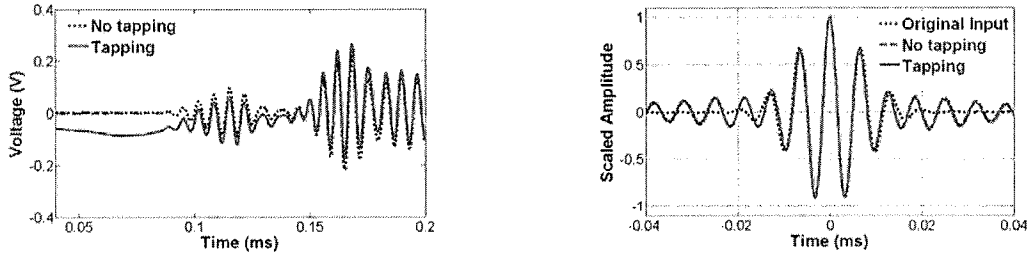

(a) Forwarding signal (b) Reconstructed signal after the TRP

FIGURE 45 Comparison between no tapping and tapping cases

TABLE 5 Damage Indices in Different Loading Conditions

	TI	SYMI
No Tapping	0.0207283	0.999920
Tapping	0.0200829	0.999343

4.4.6 Additional Layer: The Effect of Painting Layer

For steel bridge structures, preventive painting should be applied on a regular basis (often very 2 or 3 years). In this section, the effect of an additional layer or a surface condition change on the TRP is investigated. To simulate the surface condition change, industrial putty was attached on the test beam as shown in FIGURE 46. FIGURE 47 (a) indicates that the attachment of the industrial putty significantly attenuated the forwarding response signal and the dispersion characteristic was also altered. However, the shape of the reconstructed signal was preserved again [FIGURE 47 (b)]. It should be noted that the reconstructed signal shown in FIGURE 47 (b) is scaled so that it can be better compared with the original input signal. In addition, Eq. (1) shows the TR index is not affected by the amplitude difference between the original input and reconstructed signal.

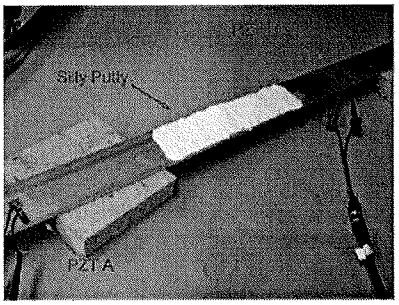

FIGURE 46 Surface condition change using an industrial silly putty

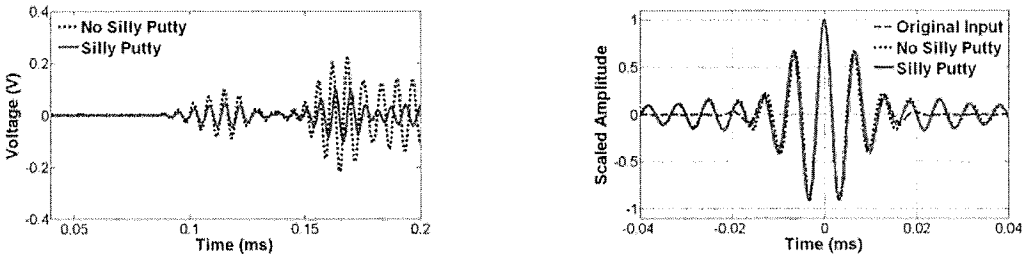

(a) Forwarding signal (b) Reconstructed signal after the TRP

FIGURE 47 Comparison between no silly putty and silly putty cases

4.5 DAMAGE DETECTION IN STIFFENER AND GIRDER CONNECTIONS

After the idea of using a PZT poling direction for crack detection was validated in a plate structure, the idea is applied to a stiffener-girder connection case in order to monitor stiffeners of a steel bridge girder. In this report, numerical

simulation is attempted using similar configuration described in 4.1 [FIGURE 48]. A 6 mm × 45 mm stiffener was placed exactly in the middle of PZT A and B (or PZT C and D), and forwarding signals from different wave paths were obtained and compared. Other conditions such as PZT size, input frequency, and input parameters are identical to the values described in 4.1. In the plate test case, signal AB was identical to signal CD. However, signals AB and CD obtained from the stiffener-girder connection were different due to the effect of stiffener [FIGURE 49 (a)]. When a propagating Lamb wave signal encounters a stiffener, some portion of the signal will be transmitted, and some will be reflected to the source location. In addition, mode conversion is occurring due to sudden thickness variation, and even some portion of the signal will propagate into the stiffener. Therefore, it can be inferred that if two wave paths are identical, the effect of the stiffener on Lamb wave propagation can be minimized. Based on the proposed piezoelectric polarization theory, signals AB and CD as well as signals AC and BD are identical in a symmetric geometry. Considering the geometry of the stiffener-girder connection, signals AC and BD have identical wave paths. As a consequence, signals AC and BD obtained from the simulation are identical [FIGURE 49 (b)]. After checking signals AC and BD, a notch with 2 mm depth and 1 mm width was created right next to the stiffener [FIGURE 48 (b)]. As illustrated in FIGURE 50, out-of-phase signals appeared due to mode conversion induced by the notch.

Next, the effect of welding between the stiffener and the web are investigated [FIGURE 51]. The dimension of the structure and variables used in the simulation are the same as the previous model except for the existence of welding. Based on the simulation result, the different welding condition at both sides of the stiffener introduced mode conversion [FIGURE 52 (a)]. Next, two different configurations were made to simulate damages around the stiffener. Configuration 1 shows the case when a welding and a defect are located on the different side [FIGURE 51 (a)]. On the other hand, the damage and the welding are on the same side in Configuration 2 [FIGURE 51 (b)]. In both cases, large out-of-phase signals due to mode conversion were generated in spite of different welding conditions [FIGURE 53 (b), FIGURE 54 (b)]. The numerical study so far indicates that the fatigue crack around the stiffener-girder connection can be monitored even at the presence of nonsymmetrical welding conditions using the proposed NDT concept in this report.

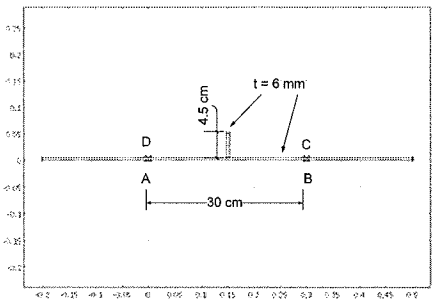

(a) Intact condition (Configuration I)

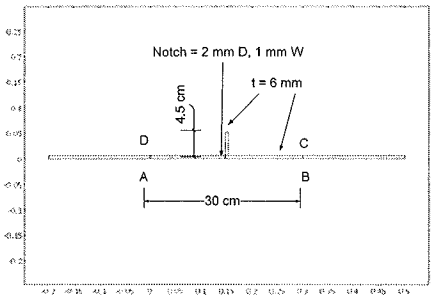

(a) Notch generated next to the stiffener (Configuration II)

FIGURE 48 Dimension of an aluminum plate with an aluminum stiffener used in numerical simulation

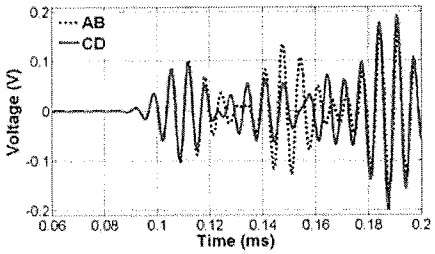

(a) Signals AB and CD without a notch (Configuration I)

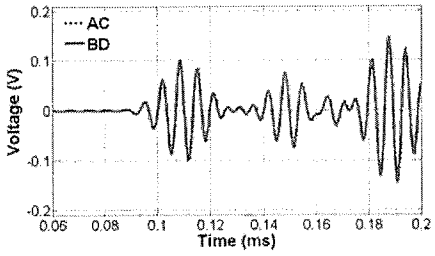

(b) Signals AC and BD without a notch (Configuration I)

FIGURE 49 Simulated Lamb wave signals without notch

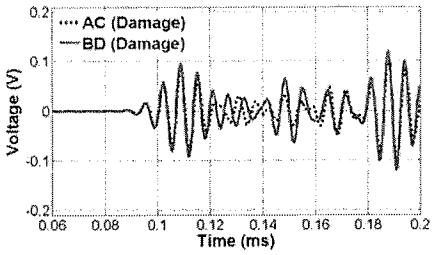

FIGURE 50 Simulated Lamb wave signals with notch (Configuration II)

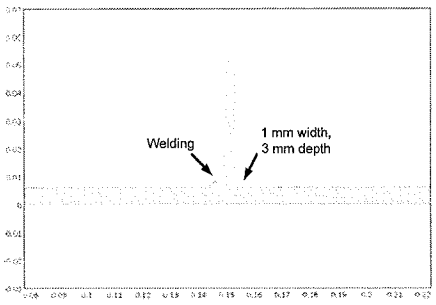

(a) Configuration I

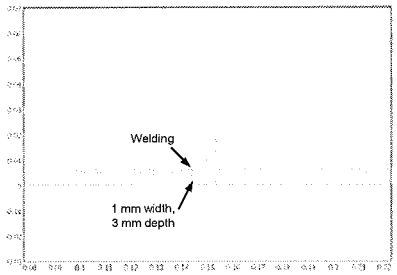

(b) Configuration II

FIGURE 51 Dimension of an aluminum plate with an aluminum stiffener used in numerical simulation

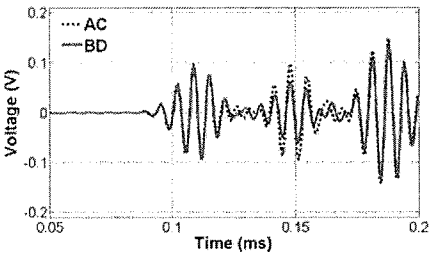

(a) Signals AC and CD without a notch

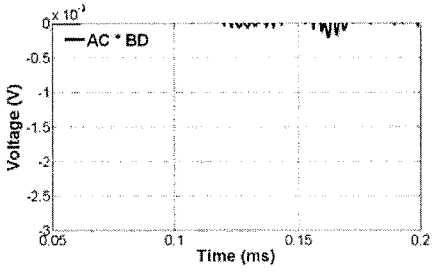

(b) The negative PPP values of signals AC and BD without a notch

FIGURE 52 Simulated Lamb wave signals without notch

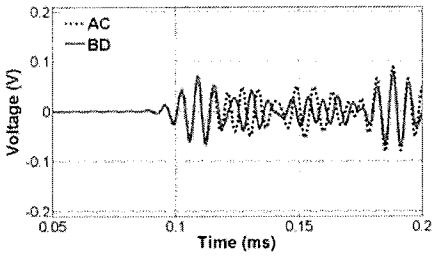

(a) Signals AB and CD with a notch (Configuration I)

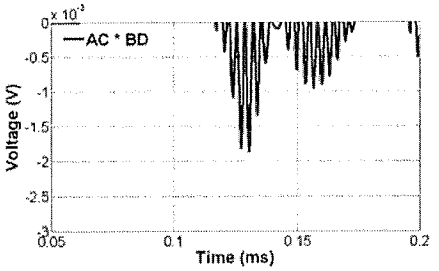

(b) The negative PPP values of signals AC and BD with a notch (Configuration I)

FIGURE 53 Simulated Lamb wave signals with a notch (Configuration I)

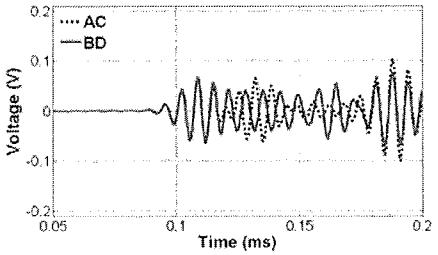

(a) Signals AB and CD with a notch (Configuration II)

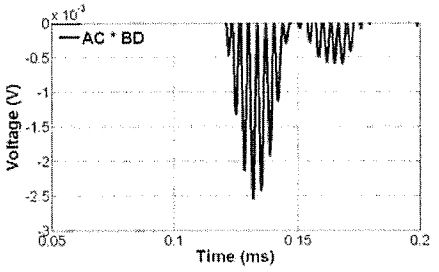

(b) The negative PPP values of signals AC and BD with a notch (Configuration II)

FIGURE 54 Simulated Lamb wave signals with a notch (Configuration II)

5. FIELD TEST RESULTS FROM THE BUFFALO CREEK BRIDGE IN PENNSYLVANIA

5.1 TEST SETUP

A preliminary field test in preparation for Stage 2 was conducted at the Buffalo Creek Bridge in Armstrong County, PA with permission from District 10 office of the Pennsylvania Department of Transportation. The buffalo Creek Bridge carries 4-lane traffic, and it is composed of a concrete deck and 12 main steel girders. A photo of the Buffalo Creek Bridge and the location of the steel girder tested are shown in FIGURE 55.

The test was conducted in one of the steel girders near the north end of the bridge supports [FIGURE 56]. The girder tested is one of the interior girders (the third one from the north-east exterior girder), and its dimension is 1.83 m height and 0.0111 m thick. In every 1.6375 m, 8mm-thick stiffeners are welded on the alternative sides of the web [FIGURE 55 (a)].

A total of five PZT transducer pairs were mounted on the tested steel girder. These five pairs are listed as Paths 1 to 5 in FIGURE 56 (a). In this test, the piezoelectricity of PZTs allows them to function as both actuators and sensors [9]. The distance between each pair of the PZTs was set to 1 m. In this experiment, a PSI-5A4E type of PZT (thickness = 0.0508 cm) was cut to a square shape (2.5 cm × 2.5 cm) and attached on the surface of the steel girder's web with a commercial cyanoacrylate adhesives. The data acquisition system consisted of an arbitrary signal generator (AWG), a high-speed signal digitizer (DIG), a low noise preamplifier (LNP), and an external power source. In order to control the data

acquisition system remotely using a laptop computer, a USB wireless modem protocol (Linksys WUSB54G) was installed in the system [FIGURE 56 (b)].

A tone-burst signal with 20 peak-to-peak voltage was generated using 14-bit AWG, and the PZTs were excited at the frequency of 100 kHz. First, PZT A in FIGURE 56 (a) was excited by this input waveform. Then, PZT A generated elastic waves, and the response was measured at PZT B. When the guided waves arrived at PZT B, the voltage output from PZT B was amplified by LNP with a gain of 20 and measured by 16-bit DIG. The sampling rate of DIG was 5 MS/sec, and resolution was ± 0.2 V. In this preliminary test, the effects of vibration due to traffic loading and the PZT grounding on Lamb wave propagation were mainly checked.

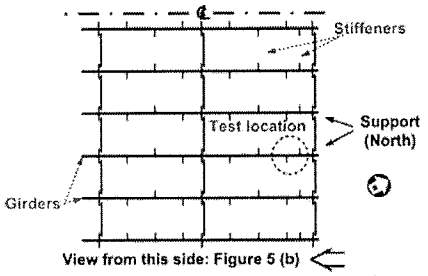

(a) Detailed drawing of the test location

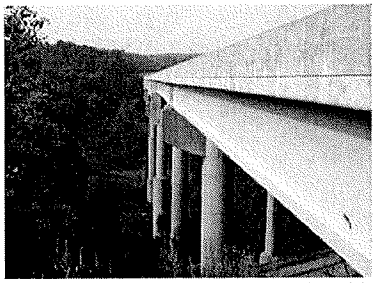
(b) Overview of the Buffalo Creek Bridge

FIGURE 55 The overview and the description of the Buffalo Creek Bridge in Pennsylvania

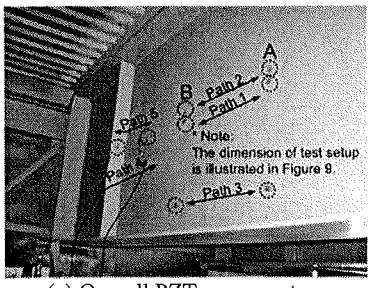

(a) Overall PZT sensor setup.

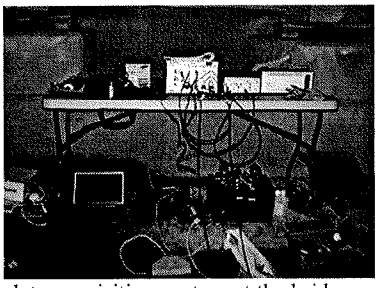
(b) A data acquisition system at the bridge support

FIGURE 56 Overall test setup configuration for Buffalo Creek Bridge testing

After the preliminary field test in Stage 1, a main field test was conducted again at the Buffalo Creek Bridge, and the same steel girder was tested as described in FIGURE 55 (a). On the test date, the traffic was not blocked, and the temperature of the site was around 1 °C . A total of three PZT transducer pairs were mounted on the steel girder tested. These PZT pairs are denoted as Configuration 1 and Configuration 2 in FIGURE 57. Configuration 1 consists of PZT A, B, C and D and PZT A, B, C', and D' are included in Configuration 2. The main difference between Configuration 1 and Configuration 2 is the existence of stiffener along the wave path [FIGURE 57]. The distance between two PZT pairs in Configuration 1 was set to 65 cm, and the distance in Configuration 2 was set to 54 cm, respectively. In this experiment, a PSI-5A4E type of PZT (thickness = 0.0508 cm) was cut to a square shape (2 cm × 2 cm) and attached on the both surfaces of the steel girder's web with a commercial cyanoacrylate adhesives. The data acquisition system in the main test included an AWG, a DIG, a LNP, a high-pass filter circuit, and an external power source.

A tone-burst signal with 20 peak-to-peak voltage was generated using 14-bit AWG, and the PZTs are excited at the frequency of 120 kHz. First, PZT A in Configuration 1 [FIGURE 57] was excited by this input waveform. Then, PZT A generated elastic waves, and the response was measured at PZT C in Configuration 1. When the guided waves arrived at PZT C, the voltage output from PZT C was filtered by the high-pass filter circuit (cut off frequency: 8 kHz). This circuit plays a roll to reduce the effect operational variation of the bridge. Even though the filtering scheme provided by the LNP and the DIG can eliminate low frequency components of the received signal, this additional circuit prevents the LNP from being overloaded. The signal after the circuit was amplified by LNP with a gain of 50 and measured by 16-bit DIG. The sampling rate of DIG was set to 20 MS/sec. Finally, the signal was filtered again using software filter proposed in Chapter 5 (a 5th order Butterworth filter with cutoff frequencies of 30 kHz to 300 kHz, gain: 5).

In this experiment, after the forwarding signal from PZT A to PZT C in Configuration 1 (signal AC) was measured, the same process was repeated by exciting PZT B and measuring response at PZT D in Configuration 1 (signal BD). Finally, the PPP values of signals AC and BD were calculated and monitored. After the forwarding Lamb wave signals were measured, the TRP was conducted. The signal AC (signal BD) was reversed in the time domain, and resent to the PZT C (PZT D). The reconstructed signal after the TRP was measured at PZT A (PZT B), and signal ACA was compared with signal BDB. Detailed test results are described in the next subsection.

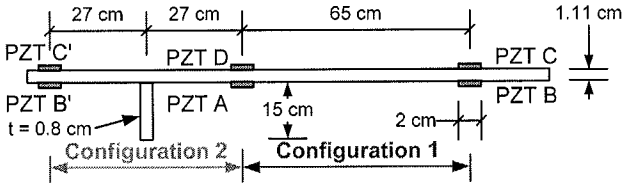

FIGURE 57 A schematic diagram of PZT setup in the field test

5.2 EXPERIMENTAL RESULTS

5.2.1 Removing Vibration Induced by Traffic Loading

Due to normal traffic on the Buffalo Creek Bridge, the vibration response of the bridge was dominated by traffic loading and it was difficult to extract Lamb wave responses produced by the PZT excitation. For instance, FIGURE 58 (a) shows a typical vibration response obtained from a pair of PZTs [Path 2 in FIGURE 59] when normal traffic was on the bridge. Note that the signal was saturated because the vibration response induced by traffic loading exceeded the dynamic range of DIG ($\pm$ 0.2 V). In order to extract the guided wave response of our interest, several filtering options were investigated. First, an analog filter built in LNP was used. This analog filter has adjustable cutoff frequency values, and the range of the band-limited filter is set to 10 to 300 kHz. It did not fully remove the dynamic response due to traffic loading. Next, the same test was repeated only using a digital filter built in LabVIEW software (a 5th order Butterworth filter with cutoff frequencies of 30 kHz to 300 kHz). As expected, the digital filter itself did not improve the response signal because the signal was already saturated even before applying the digital filter. Finally, when both analog and digital filters were applied to the response signal, the Lamb wave response was successfully extracted as shown in FIGURE 58 (b). Finally, to improve the signal to noise ratio, the same input waveform was repeatedly applied 5 times, and the corresponding responses were averaged in the time domain.

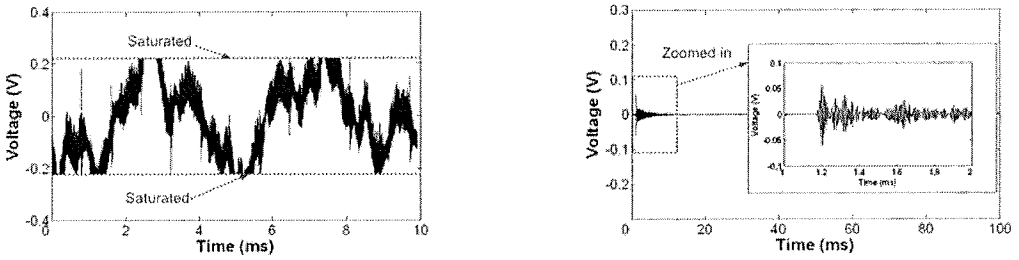

(a) Without any filtering (b) With both analog and digital filtering

FIGURE 58 Removal of the dynamic vibration induced by traffic loading using analog and digital filtering

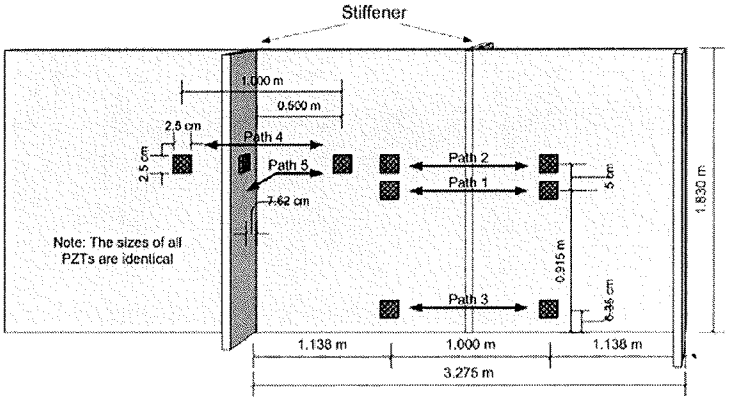

FIGURE 59 Dimension of a girder, sensor array setup, and the notation of each test case

5.2.2 Grounding of PZT Patches

The effect of the PZT grounding condition on Lamb wave propagation is investigated by examining response signals obtained from three different PZT pairs: Paths 1 to 3 in FIGURE 59. For Path 1 case, PZTs were simply mounted on the painted surface of the steel girder without any special treatment. PZTs were mounted in the exactly same fashion in Path 2 case except that the steel girder is properly grounded to provide a common-mode ground for both PZTs. In Path 3 case, the painting layer was removed before PZT attachment and the steel girder is grounded. FIGURE 60 (a) shows that, without proper grounding, the subtle Lamb wave responses are masked by much larger electro-mechanical interference (EMI). With proper grounding in Path 2 case, the EMI is reduced as shown in FIGURE 60 (b). Finally, the EMI is completely removed in Path 3 case shown in FIGURE 60 (c). Note that the fluctuation of the signal in Path 3 case is mainly caused by the dynamic vibrations induced by traffic loading. However, removing the painting layers is labor intensive, and the spot can be vulnerable to corrosion. Instead, a digital filter previously described was selected to remove both EMI and traffic-induced vibrations.

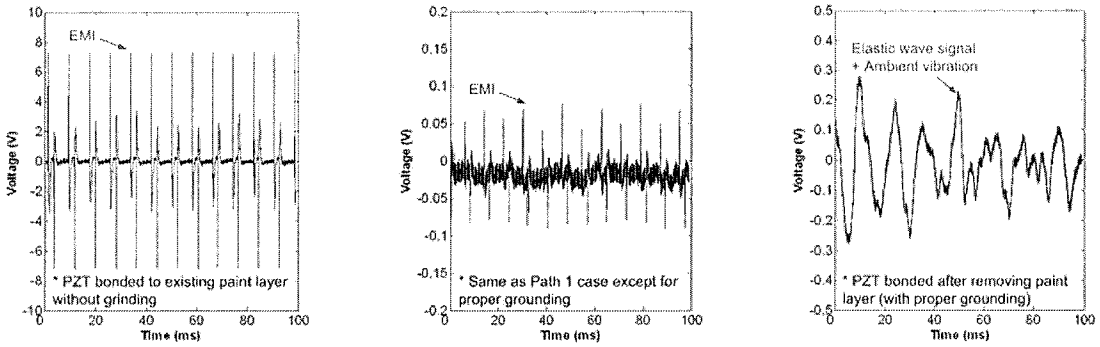

(a) Path 1 (b) Path 2 (c) Path 3

FIGURE 60 Measured signals from sensor pairs with different bonding conditions
(Analog filtering only, Definition of Path 1 to 3 are shown in FIGURE 59)

5.2.3 Test on a web of the girder (Configuration 1)

In FIGURE 61 (a), Lamb wave signals obtained from a web of the girder are presented [Configuration 1 in FIGURE 57]. Using the test setup described in 5.1, signals AC and BD were measured. Although signal AC was supposed to be identical to signal BD, differences between signals AC and BD were observed in FIGURE 61 (b) due to imperfections in PZT alignment, size and bonding condition. Then, the proposed thresholding technique was applied to the PPP values between signals AC and BD. Using the proposed thresholding technique, the negative PPP values resulted only from the mode conversion should remain while the negative values associated with the sensor misalignment should have been selectively removed. As shown in FIGURE 63 (a), the negative PPP values between signals AC and BD were negligible at the absence of a notch [FIGURE 63 (a)].

Next, the same procedure was conducted using reconstructed signals after the TRP. FIGURE 62 (a) clearly shows that the two reconstructed signals were almost identical without defect on the girder. The deviation of the two reconstructed signals from original input signal is shown in TABLE 6. As shown in TABLE 6, low TI values and high SYMI values of the both reconstructed signals indicate that the TRP were successfully conducted. After the TI and SYMI were computed for each case, the negative PPP values between signals ACA and BDB were calculated in a manner similar to the ones between signals AC and BD. By applying the thresholding technique, the negative PPP values between ACA and BDB became negligible as well [FIGURE 63 (b)]. Throughout the test on the web (Configuration 1), the applicability of the proposed method to the field structures was clearly shown. In the next subsection, the Lamb wave propagation as well as the TRP along a stiffener-girder connection is tested.

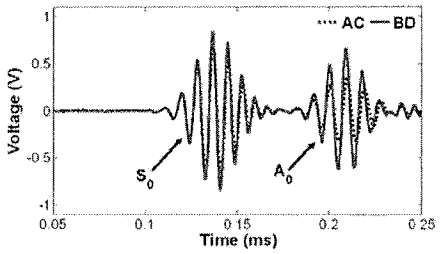

(a) Signals AC and BD in Configuration 1

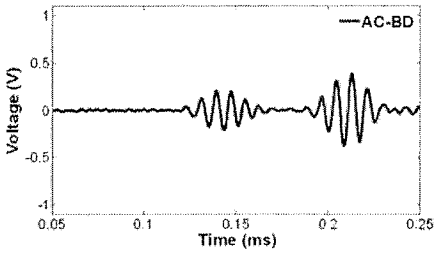

(b) Difference between signals AC and BD

FIGURE 61 Comparison of signals AB and CD in Configuration 1

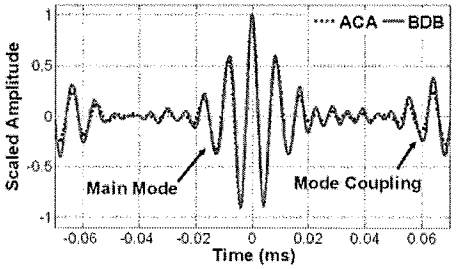

(a) Signals ABA and CDC in Configuration 1

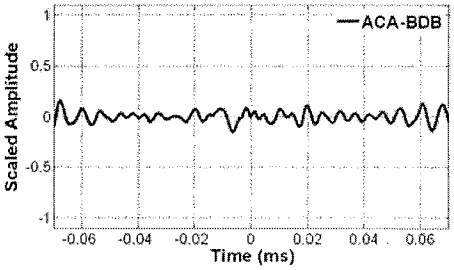

(b) Difference between signals ABA and CDC

FIGURE 62 Comparison of signals ABA and CDC in Configuration 1

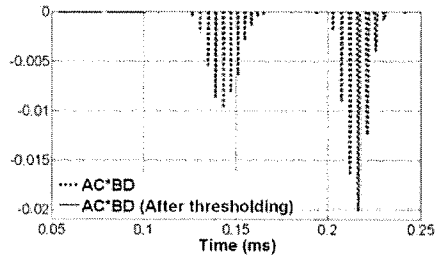

(a) Negative PPP values between signals AC and BD before and after applying the proposed thresholding

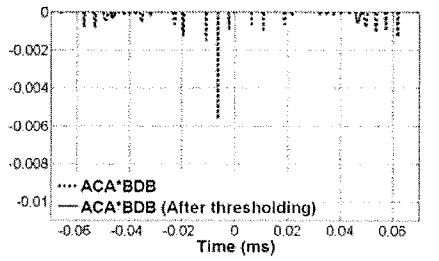

(b) Negative PPP values between signals ACA and BDB before and after applying the proposed thresholding

FIGURE 63 Negative PPP values between signals AC (ACA) and BD (BDB) before and after applying the proposed thresholding (Configuration 1)

TABLE 6 Damage Indices in Different Loading Conditions

	TI	SYMI
ACA	0.0200484	0.991061
BDB	0.0144714	0.992557

5.2.4 A stiffener-girder connection test (Configuration 2)

Previously in section 4.5, a numerical study simulating Lamb wave propagation along a stiffener-girder connection is attempted. In this subsection, the numerical simulation in 4.5 was verified experimentally. As stated previously, not only signals AB and CD but also signals AC and BD should be identical at the absence of defects in the plate test case. However, only signals AC and BD will be identical in the stiffener-girder connection because of the mode conversion

induced by its complex geometry. In order to check the theoretical approach, signals AC' and BD' in Configuration 2 were measured using the test setup described in 5.1. In the test using Configuration 1, either S_0 mode or A_0 mode in signals AC and BD arrived at the same time that signals AC and BD could be examined without any adjustment. On the other hand, S_0 mode and A_0 modes in signals AC' and BD' were slightly mismatched in the time domain due to sensor misalignment in Configuration 2. To reduce this effect of time delay in signals AC' and BD', signal AC' was shifted to the left until their difference was minimized. [FIGURE 64 (a), (b)]. Based on the simulation result in 4.5, the signal AC' was supposed to be identical to the signal BD'. However, mode converted signals were shown between S_0 and A_0 modes in this test case [FIGURE 64 (a)]. Even after applying thresholding technique to the negative PPP values between signals AC' and BD', the signal due to mode conversion remained [FIGURE 66 (a)]. The effect of mode conversion was also shown clearly in the reconstructed signals after the TRP [FIGURE 65, FIGURE 66].

When Lamb wave signals are generated at PZT A, some portion of the signals will propagate along the girder, and some will travel through the stiffener and travel back to the girder again. Moreover, mode conversion happens around the connection between the stiffener and the plate. In case the stiffener is located exactly in the middle of the PZTs and the both sides of the stiffener is identically welded, signals AC' and BD' should be identical to each other because the setup is exactly symmetrical along the stiffener. Therefore, it can be inferred that the difference between signals AC' and BD' are induced by either sensor misalignment or different welding condition. Even though simulation results in 4.5 showed that the fatigue crack can be monitored even at the presence of nonsymmetrical welding conditions, more research is required to differentiate the effect of damage from sensor misalignment or different welding condition.

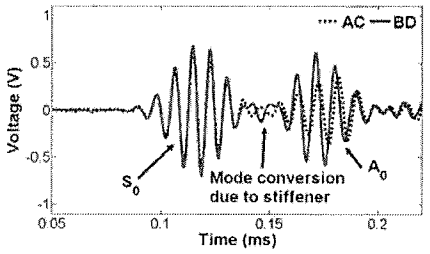

(a) Signals AC and BD in Configuration 2

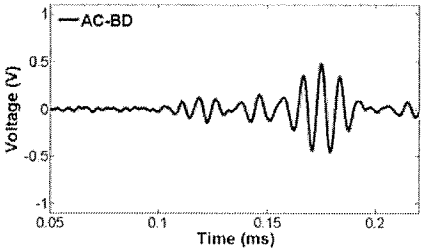

(b) Difference between signals AC and BD

FIGURE 64 Comparison of signals AB and CD in Configuration 2
(Signal AC was shifted to the left to minimize AC-BD)

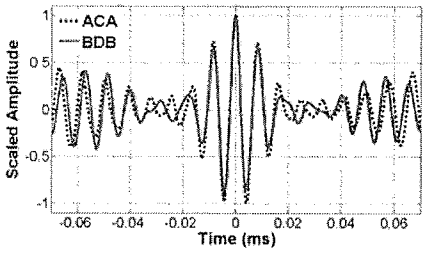

(a) Signals ABA and CDC in Configuration 2

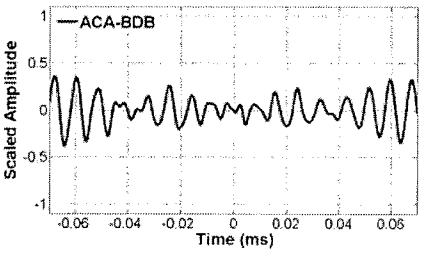

(b) Difference between signals ABA and CDC

FIGURE 65 Comparison of signals ABA and CDC in Configuration 2

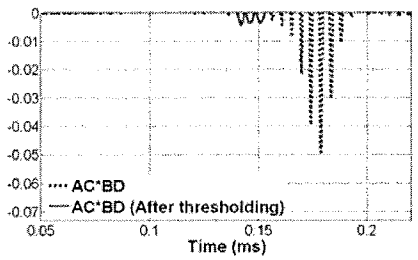

(a) Negative PPP values between signals AC and BD before and after applying the proposed thresholding

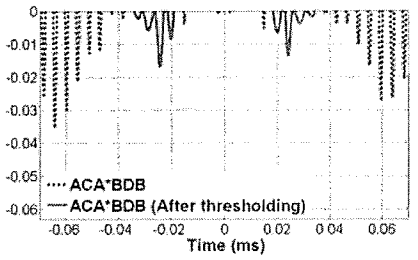

(b) Negative PPP values between signals ACA and BDB before and after applying the proposed thresholding

FIGURE 66 Negative PPP values between signals AC (ACA) and BD (BDB) before and after applying the proposed thresholding (Configuration 2)

5.3 ISSUES RELATED TO FIELD IMPLEMENTATION

In this report, a NDT technique which is applicable to real bridge structures is developed. In order to apply this technique to field bridge structures, there are several practical implementation issues needed to be addressed.

I. PZT fabrication: The NDT technique proposed in this study is based on the usage of PZT transducers. As described in Chap 4, elastic waves propagating along steel girders of field bridges are sensitive to the condition of PZT transducers. Therefore, precise fabrication of each PZT transducer should be guaranteed first. In this study, PZT transducers are fabricated by tailoring a commercial PZT patch (7.24 mm by 7.24 mm, $ 60) into small wafer transducers manually. It is expected that manufacturing PZT transducers can reduce variations in PZT size so that the effect of PZT imperfection described in 4.4.2 can be prevented.

II. PZT installation: It must be noted that the proper attachment of PZT transducers are critical for the field implementation of the technique. When a PZT transducer is mounted, it should be firmly pressed so that a bonding layer between the transducer and a steel girder is not too thick. Also, even though PZT transducers can be directly attached to the painting layer of girders, the surface of the layer must be smooth enough to provide proper bonding condition. For long term monitoring, sealing PZT transducers using acrylic epoxy might be helpful to protect PZT transducers from harsh environment.

III. Ambient traffic loading: In 5.2.1, the effect of ambient vibration due to traffic loading is shown. A low frequency vibration induced by traffic loading affects measured a Lamb wave signal so that the amplitude of the signal exceeds the input range of data acquisition devices. Since the frequency range of Lamb waves used in this research is much higher (50 kHz to 200 kHz) than the traffic loading (30 – 100 Hz), a simple high-pass filter circuit can alleviate the effect of ambient vibration.

IV. Wiring: The proposed NDT can be applied to a field bridge after all transducers are properly mounted to the target bridge and the effect of ambient vibration is removed. At the current stage, transducers are wired to data acquisition devices so that the power supply and signal measurement is conducted using cables. Now, a research is being investigated as a future work in order to provide power to PZT transducers and receive signals at the same time using wireless technique.

6. CONCLUSION

A new concept of reference-free NDT is being investigated based on the premise that "certain types of damage can be instantaneously detected without using prior baseline data." In this study, the theoretical frame of the proposed baseline-free NDT technique, a time reversal process (TRP), was developed and a NDT methodology for detecting cracks in steel girders commonly used in bridges was formulated. So far, the specific questions in Stages 1 and 2 such as (1) sensing range of the proposed TRP, (2) the effects of different types of flaws on the TRP, (3) the effect of sensor bonding condition, and (4) the effects of operational and environmental variations are validated through controlled laboratory experiments. In this research, the sensing range of the TRP and the effects of different types of damage on the TRP are investigated first. Waves generated by test setup propagate about 40 m in one dimensional test, and not only a foreign object but also a notch along wave path is separately detected using the TRP. Especially, by attaching one more PZT pair considering poling directions of the PZTs, only the mode converted signal due to damage were successfully extracted from two measured reconstructed signals. In addition, from extracted signals, the possible locations of crack damage were determined as well. Using numerical simulation, the Lamb wave propagation in a complex geometry is investigated. Next, in order to address sensor defect issues, a novel method which can detect sensor debonding and cracking is introduced. In this report, the robustness of the TRP against environmental and operational variation is verified experimentally. Laboratory experiments are conducted to demonstrate that the proposed NDT technique is not significantly influenced by (1) ambient temperature variations, (2) imperfect sizing and positioning of the active sensing devices, (3) ambient background vibration of the test specimens, (4) changes of the test specimen's boundary conditions, and (5) surface debris or additional painting layer on the steel girders. Finally a field test was conducted at one of local bridges in Pennsylvania. In the field test, it has been shown that the proposed NDT methods including the TRP may be applicable to field bridge monitoring. It was demonstrated that cracks in the main girders and the girder-stiffener connections could be potentially detected even at the presence of traffic loading, temperature changes, and variation in PTZ conditions. However, further research is warranted to make technology transition to commercial applications.

7. REFERENCES

1. M. Fink, "Time-reversed acoustics", *Scientific American*, Vol. 281, No. 5, 1999, pp. 91-97.
2. R. K. Ing, M. Fink, "Time recompression of dispersive Lamb waves using a time reversal mirror – Application to flaw detection in thin plates", *IEEE Ultrasonics Symposium*, No. 1, 1996, pp. 659-663.
3. S. B. Kim, H. Sohn, D. W. Greve, I. J. Oppenheim, "Application of a time reversal process for baseline-free monitoring of a bridge steel girder", *International Workshop on Structural Health Monitoring*, Stanford, CA, September 15-17, 2005.
4. H. Sohn, S. B. Kim and H. W. Park, "Searching for a reference-free damage detection technique", *The Second International Workshop on Advanced Smart Materials and Smart Structures Technology*, 2006.
5. S. D. Kim, C. W. In, K. E. Cronin, H. Sohn and K. Harries, "Active sensing for Disbond Detection in CFRP strengthened RC beam", *European SHM*, 2006.
6. I. Viktorov, Rayleigh and Lamb Waves, Plenum Press: New York, 1967.

7. C. Prada and M. Fink, "Separation of interfering acoustic scattered signals using the invariants of the time-reversal operator. Application to Lamb waves characterization", *Journal of the Acoustical Society of America*, Vol. 104, No. 2, 1998, pp. 801–807.

8. R. Ing and M. Fink, "Time-reversed Lamb waves", *IEEE transactions on ultrasonics, ferroelectrics, and frequency control*, Vol. 45, No. 4, 1998, pp. 1032-1043.

9. V. Giurgiutiu and A. N. Zagrai, "Characterization of piezoelectric wafer active sensors," Journal of Intelligent Material Systems and Structures, Vol. 11, No. 12, 2000, pp. 959-976.

10. C. H. Wang, J. T. Rose and F. K. Chang, "A synthetic time-reversal imaging method for structural health monitoring", *Smart Material and Structures*, Vol. 13, No. 2, 2004, pp. 415-423.

11. J. Fraden, Handbook of Modern Sensors, American Institute of Physics, 2nd Edition, 2001.

12. R. C. Buchanan, Ceramic Materials for Electronics, 3rd Edition, 2004.

13. Z. Su and L. Ye, "Selective generation of Lamb wave modes and their propagation characteristics in defective composite laminates", *Proceedings of the Institution of Mechanical Engineers, Part L: Journal of Materials: Design and Applications*, Vol. 218, No. 2, 2004,pp. 95-110.

14. Y. Cho, "Estimation of ultrasonic guided wave mode conversion in a plate with thickness variation", *IEEE transactions on ultrasonics, ferroelectrics, and frequency control*, Vol. 47, No. 3, 2000, pp. 591-603.

15. H. W. Park, S. B. Kim and H. Sohn, "Understanding a Time Reversal Process in Lamb Wave Propagations", *In preparation for Journal of Sound and Vibration*, 2007.

16. V. Giurgiutiu, "Tuned Lamb-wave excitation and detection with piezoelectric wafer active sensors for structural health monitoring", Journal of Intelligent Material Systems and Structures, Vol. 16, No. 4, 2005, pp. 291-306.

17. COMSOL AB, COMSOL Multiphysics User's Guide, Version 3.2, 2005.

18. S. Lee and H. Sohn, "Self-sensing scheme development for differentiating sensor detect from structural damage", *Proceedings of ASME International Mechanical Engineering Congress and Exposition*, 2006.

19. A. H. Nayfeh and P. F. Pai, 2004, Linear and Nonlinear Structural Mechanics, Wiley-Interscience: New York, 2004.